Title

Emerging Trends in Heart Valve Engineering: Part IV. Computational Modeling and Experimental Studies

Journal

Annals of Biomedical Engineering, 43(10)

ISSN

0090-6964

Authors

Kheradvar, A
Groves, EM
Falahatpisheh, A
et al.

Publication Date

2015-10-22

DOI

10.1007/s10439-015-1394-4

Peer reviewed

Annals of Biomedical Engineering (© 2015)
DOI: 10.1007/s10439-015-1394-4

Emerging Trends in Heart Valve Engineering: Part IV. Computational Modeling and Experimental Studies

ARASH KHERADVAR,[1,2] ELLIOTT M. GROVES,[1,2] AHMAD FALAHATPISHEH,[1] MOHAMMAD K. MOFRAD,[3] S. HAMED ALAVI,[1] ROBERT TRANQUILLO,[4] LAKSHMI P. DASI,[5] CRAIG A. SIMMONS,[6,7] K. JANE GRANDE-ALLEN,[8] CRAIG J. GOERGEN,[9] FRANK BAAIJENS,[10] STEPHEN H. LITTLE,[11] SUNCICA CANIC,[12] and BOYCE GRIFFITH[13,14]

[1]Department of Biomedical Engineering, The Edwards Lifesciences Center for Advanced Cardiovascular Technology, University of California, Irvine, 2410 Engineering Hall, Irvine, CA 92697-2730, USA; [2]Department of Medicine, Division of Cardiology, University of California, Irvine School of Medicine, Irvine, CA, USA; [3]Department of Bioengineering and Mechanical Engineering, University of California, Berkeley, CA, USA; [4]Department of Biomedical Engineering, University of Minnesota, Minneapolis, MN, USA; [5]Department of Mechanical Engineering, School of Biomedical Engineering, Colorado State University, Fort Collins, CO, USA; [6]Department of Mechanical & Industrial Engineering, University of Toronto, Toronto, ON, Canada; [7]Institute of Biomaterials & Biomedical Engineering, University of Toronto, Toronto, ON, Canada; [8]Department of Bioengineering, Rice University, Houston, TX, USA; [9]Weldon School of Biomedical Engineering, Purdue University, West Lafayette, IN, USA; [10]Department of Biomedical Engineering, Eindhoven University of Technology, Eindhoven, The Netherlands; [11]Houston Methodist DeBakey Heart & Vascular Center, Houston, TX, USA; [12]Department of Mathematics, University of Houston, Houston, TX, USA; [13]Department of Mathematics, Center for Interdisciplinary Applied Mathematics, University of North Carolina at Chapel Hill, Chapel Hill, NC, USA; and [14]McAllister Heart Institute, University of North Carolina at Chapel Hill School of Medicine, Chapel Hill, NC, USA

(*Received 26 April 2015; accepted 14 July 2015*)

Associate Editor K. A. Athanasiou oversaw the review of this article.

Abstract—In this final portion of an extensive review of heart valve engineering, we focus on the computational methods and experimental studies related to heart valves. The discussion begins with a thorough review of computational modeling and the governing equations of fluid and structural interaction. We then move onto multiscale and disease specific modeling. Finally, advanced methods related to *in vitro* testing of the heart valves are reviewed. This section of the review series is intended to illustrate application of computational methods and experimental studies and their interrelation for studying heart valves.

Keywords—Computational modeling, Heart valves, Particle image velocimetry, Biaxial testing, Multiscale modeling, Numerical simulation.

INTRODUCTION

Over the past two decades, computational modeling and experimental studies have been used as powerful tools to understand and predict the behavior and mechanics of native and prosthetic heart valves in normal and pathological conditions. These studies have aided the assessment of heart valves, interventional and surgical procedures, heart valve design, and general understanding of healthy and abnormal cardiac valve function.

To be viable, computational models must be evidently based on an accurate representation of the mechanical behavior of the valves' material and flow passing through the valves. Native heart valve leaflet tissue has many important biomechanical attributes contributing to its elastic response to the loads along with a viscous reaction that damps out flow-related vibrations, making its overall response as viscoelastic. Nonetheless, water comprises a major fraction of the collagenous tissue by weight and is tightly bound to the fibrous network; hence the heart valve tissue behaves nearly or completely incompressible. Moreover, the aligned fibers of the leaflet tissue make the stress–strain response highly anisotropic.[14] The waviness of the fibers also significantly affects the stress–strain response.[156] A constitutive model for heart valve tissue must incorporate important features of the heart valves. Namely it should describe a pseudoelastic, incompressible, anisotropic, nonlinear material. Extensive work has been devoted to developing constitutive equations to describe the mechanics of the heart valve leaflet tissues.[119,144,156,157,159] Different derivations for the stress–strain behavior of the heart valves have been attempted, which treat the structure of the native tissue using

Address correspondence to Arash Kheradvar, Department of Biomedical Engineering, The Edwards Lifesciences Center for Advanced Cardiovascular Technology, University of California, Irvine, 2410 Engineering Hall, Irvine, CA 92697-2730, USA. Electronic mail: arashkh@uci.edu

Published online: 30 July 2015

different approaches ranging from phenomological models that include no information about the structure to unit-cell models that are completely derived from network structure as extensively described by Weinberg and Kaazempur-Mofrad.[156]

In this final section of a four-part review series, we focus on the various aspects of computational modeling and experimental studies related to heart valves. Ranging from pure computational models to *in vitro* studies, modeling is an important component of the armamentarium of those who study and design heart valves.

COMPUTATIONAL MODELING

Native and prosthetic valve leaflets are thin, flexible structures that are passively carried by the blood flow while also applying forces to the blood that affect the fluid motion and, thereby, the motion of the leaflets themselves. Static or quasi-static valve models can be used to study the mechanics of native and prosthetic valve leaflets, and standard computational fluid dynamics (CFD) approaches can be applied to study the flow patterns and fluid stresses resulting from imposed or measured leaflet kinematics.[132] Alternatively, predicting the kinematics of the valve leaflets, or the dynamic interaction between the valve leaflets and flow, requires a fluid–structure interaction (FSI) approach. Such dynamic models can be used to simulate the conditions that ultimately lead to the deterioration of the bioprosthetic valve leaflets, and validated FSI models could thereby be used to help to develop improved leaflet designs with durable lifetimes that are longer than present bioprosthetic valves.

Several computational challenges must be addressed when developing FSI models of heart valves. For instance, the valve leaflets experience large displacements and strains during the cardiac cycle. Further, FSI models that seek to model realistic loading of the closed valve must account for contact between the leaflets. Native and bioprosthetic valve leaflets generally exhibit a complex, nonlinear stress response that requires mathematical formulations appropriate for finite-strain structural models. Finally, the high Reynolds number flows characteristic of the heart valves, especially the aortic and pulmonary valves, generally necessitates the use of very high spatial resolution to resolve the flow features. Despite substantial work over several decades, the development of computational approaches that address all of these challenges remains an area of active investigation.

Governing Equations

The same fundamental equations of fluid–solid interaction can be used to describe the dynamics of native, bioprosthetic, and even mechanical heart valves. Let $\Omega \subset \mathbb{R}^3$ denote the computational domain, with $\Omega^f(t) \subset \Omega$ indicating the physical region occupied by the fluid at time t, $\Omega^s(t) \subset \Omega$ indicating the physical region occupied by the solid, and $\Omega = \Omega^f(t) \cup \Omega^s(t)$. The fluid–structure interface is $\Gamma^{fs}(t) = \Gamma^f(t) \cap \Gamma^s(t)$, in which $\Gamma^s(t)$ is the boundary of $\Omega^s(t)$ and $\Gamma^f(t)$ is the boundary of $\Omega^f(t)$. Finally, let $\boldsymbol{u}^f(\boldsymbol{x}, t)$ be the velocity of the fluid at position $\boldsymbol{x} \in \Omega^f(t)$ at time t, and let $\boldsymbol{u}^s(\boldsymbol{x}, t)$ be the velocity of the structure at position $\boldsymbol{x} \in \Omega^s(t)$ at time t. To simplify notation, we shall generally omit the superscripts "f" and "s" on the velocity field. Instead, we identify $\boldsymbol{u}(\boldsymbol{x}, t)$ as the velocity of whichever material happens to be located at position $\boldsymbol{x}$ at time t.

The equations of momentum conservation for the fluid and solid are:

$$\rho^f \frac{D\boldsymbol{u}}{Dt}(\boldsymbol{x}, t) = \nabla \cdot \boldsymbol{\sigma}^f(x, t) \quad \text{in} \quad \Omega^f(t), \tag{1}$$

$$\rho^s \frac{D\boldsymbol{u}}{Dt}(\boldsymbol{x}, t) = \nabla \cdot \boldsymbol{\sigma}^s(\boldsymbol{x}, t) \quad \text{in} \quad \Omega^s(t), \tag{2}$$

in which ρ^f and ρ^s are, respectively, the mass densities of the fluid and solid, $\boldsymbol{\sigma}^f(\boldsymbol{x}, t)$ and $\boldsymbol{\sigma}^s(\boldsymbol{x}, t)$ are the (Cauchy) stress tensors of the fluid and the solid, and $\frac{D(\cdot)}{Dt} = \frac{\partial(\cdot)}{\partial t} + \boldsymbol{u}(\boldsymbol{x}, t) \cdot \nabla(\cdot)$ is the material (convective) time derivative. The fluid and structure may both be modeled as incompressible, so that

$$\nabla \cdot \boldsymbol{u}(\boldsymbol{x}, t) = 0. \tag{3}$$

Typical coupling conditions for the fluid and structure regions are that of the velocity and traction, and are continuous along $\Gamma^{fs}(t)$, i.e.,

$$\boldsymbol{u}^f(\boldsymbol{x}, t) = \boldsymbol{u}^s(\boldsymbol{x}, t) \quad \text{on} \quad \Gamma^{fs}(t), \tag{4}$$

$$\boldsymbol{\sigma}^f(\boldsymbol{x}, t) \cdot \boldsymbol{n} = \boldsymbol{\sigma}^s(\boldsymbol{x}, t) \cdot \boldsymbol{n} \quad \text{on} \quad \Gamma^{fs}(t), \tag{5}$$

in which $\boldsymbol{n}$ is a unit normal vector along $\Gamma^{fs}(t)$. Boundary and initial conditions, which we omit here, are required to complete the specification of the equations of motion.

Modeling the Fluid

For the flows in the vicinity of the heart valves, blood is typically described as an incompressible Newtonian fluid, so that the fluid stress tensor is

$$\boldsymbol{\sigma}^f(\boldsymbol{x}, t) = -p(\boldsymbol{x}, t)\mathbb{I} + \mu\left(\nabla \mathbf{u}(\boldsymbol{x}, t) + \nabla \boldsymbol{u}^T(\boldsymbol{x}, t)\right), \tag{6}$$

in which μ is the (constant) dynamic viscosity of the fluid and $p(\boldsymbol{x}, t)$ is the pressure. In this case, the dynamics of the fluid in $\Omega^f(t)$ are modeled by the incompressible Navier–Stokes equations,

$$\rho^f \frac{D\boldsymbol{u}}{Dt}(\boldsymbol{x}, t) = -\nabla p(\boldsymbol{x}, t) + \mu \nabla^2 \boldsymbol{u}(\boldsymbol{x}, t), \tag{7}$$

$$\nabla \cdot \boldsymbol{u}(\boldsymbol{x}, t) = 0. \tag{8}$$

This assumption is generally sound because flow through the heart valves entails to higher Reynolds numbers (greater than 1000), therefore, granularity of the blood and other non-Newtonian characteristics of the blood can be neglected. However, it is important to consider that flow through the heart valve in fetal and embryonic stages may require considering the non-Newtonian properties of the blood since the ratio of the size of the red blood cell (RBC) to the valve lumen could be high, depending on the developmental stage. Furthermore, various generalized Newtonian and fully non-Newtonian models have been proposed [25] to describe the shear-thinning and viscoelastic properties of blood.[22,150,151] To date, the use of non-Newtonian descriptions of blood in adult models of heart valve dynamics has been somewhat limited. CFD simulations of blood flow through mechanical valves have been performed that describe blood as a power-law fluid,[5,166] a particular type of generalized Newtonian model that can capture the shear-thinning properties of blood.

Structural Modeling

Native and bioprosthetic heart valve leaflets undergo large structural deformations, making it appropriate to use a nonlinear continuum mechanics framework[69,120] to describe their material response.[69,120] Let $\boldsymbol{X}$ denote material coordinates on the leaflets in a reference configuration, which without loss of generality, we take to be the initial configuration, $\Omega_s^0 = \Omega^s(t)|_{t=0}$. The physical position of material point $\boldsymbol{X}$ at the time t is denoted $\boldsymbol{\chi}(\boldsymbol{X}, \mathrm{t}) \in \Omega^s(t)$. Because $\boldsymbol{u}(\boldsymbol{x}, t)$ is the velocity of the material at position $\boldsymbol{x}$ at time,

$$\frac{\partial \boldsymbol{\chi}}{\partial t}(\boldsymbol{X}, t) = \boldsymbol{u}(\boldsymbol{\chi}(\boldsymbol{X}, t), t). \tag{9}$$

Let $J(\boldsymbol{X}, t) = \det(\mathbb{F}(\boldsymbol{X}, t))$ be the determinant of the deformation gradient tensor $\mathbb{F}(\boldsymbol{X}, t) = \frac{\partial \boldsymbol{\chi}}{\partial \boldsymbol{X}}(\boldsymbol{X}, t)$. Because $\nabla \cdot \boldsymbol{u}(\boldsymbol{x}, t) = 0$, $\frac{\partial J}{\partial t}(\boldsymbol{X}, t) = 0$, and because the reference coordinates are taken to be the initial coordinates, the incompressibility constraint implies that $J(\boldsymbol{X}, t) = 1$ for all t.

At least over the time scale of the cardiac cycle, bioprosthetic valve leaflets can be well approximated as hyperelastic (over much longer time scales, it is necessary to adopt a description that can account for leaflet deterioration). The material response of a hyperelastic material is characterized by a strain-energy functional $W(\mathbb{F})$ of the deformation gradient $\mathbb{F}$. The corresponding first Piola–Kirchhoff stress tensor is[69,120]

$$\mathbb{P}(\boldsymbol{X}, \mathrm{t}) = \frac{\partial W}{\partial \mathbb{F}}(\boldsymbol{X}, \mathrm{t}). \tag{10}$$

The Cauchy stress $\boldsymbol{\sigma}^s(\boldsymbol{x}, t)$ is related to $\mathbb{P}(\boldsymbol{X}, t)$ *via*

$$\boldsymbol{\sigma}^s(\boldsymbol{x}, t) = -p(\boldsymbol{x}, t)\mathbb{I} + \frac{1}{J}\mathbb{P}\left(\boldsymbol{\chi}^{-1}(\boldsymbol{x}, t), t\right)\mathbb{F}^T(\boldsymbol{\chi}^{-1}(\boldsymbol{x}, t)), \tag{11}$$

in which $p(\boldsymbol{x}, t)$ is a Lagrange multiplier for the incompressibility constraint and $\boldsymbol{\chi}^{-1}(\boldsymbol{x}, t)$ is the material coordinate corresponding to physical coordinate $\boldsymbol{x}$ at time t. Various strain-energy functionals have been developed to describe heart valves,[156] including native[106] and bioprosthetic[84,85] valve leaflets. To determine the stress distribution within the leaflets in a static or quasi-static configuration, the fluid dynamics and the momentum of the solid may be neglected to solve the equilibrium problem:

$$\nabla \cdot \boldsymbol{\sigma}^s(\boldsymbol{x}, t) = 0 \quad \text{in} \quad \Omega^s. \tag{12}$$

In this case, fluid loading would appear as boundary conditions on Γ^s. For thin structures such as valve leaflets, it may be more efficient to describe the mechanics and kinematics using shell theories,[7] although a review of such descriptions is beyond the scope of this article.

In case of a mechanical valve, the kinematics of the leaflets is, to an excellent approximation, those of a rigid body. For such a body, the velocity is given by:

$$\boldsymbol{u}(\boldsymbol{x}, t) = \boldsymbol{U}(t) + \boldsymbol{W}(t) \times \boldsymbol{x}, \tag{13}$$

in which $\boldsymbol{U}(t)$ and $\boldsymbol{W}(t)$ are the linear and angular velocities of the rigid body, respectively. For these kinematics, the rate of strain tensor $\boldsymbol{d}[\boldsymbol{u}](\boldsymbol{x}, t) = \frac{1}{2}(\nabla \boldsymbol{u}(\boldsymbol{x}, t) + \nabla \boldsymbol{u}^T(\boldsymbol{x}, t))$ satisfies

$$\boldsymbol{d}[\boldsymbol{u}](\boldsymbol{x}, t) = 0. \tag{14}$$

For a rigid body, the structural stress $\boldsymbol{\sigma}^s(\boldsymbol{x}, t)$ becomes a Lagrange multiplier for the rigidity constraint $\boldsymbol{d}[\boldsymbol{u}](\boldsymbol{x}, t) = 0$,[122,143] just as $p(\boldsymbol{x}, t)$ is a Lagrange multiplier for the incompressibility constraint $\nabla \cdot \boldsymbol{u}(\boldsymbol{x}, t) = 0$. Stated more informally, the solid stress $\boldsymbol{\sigma}^s(\boldsymbol{x}, t)$ takes whatever value needed to ensure that the structure moves as a rigid body.

Numerical Methods

Approaches to simulating FSI may be roughly grouped into techniques that employ body-fitted grids for the fluid and structure, and methods that use nonconforming discretizations of the fluid and structure. Perhaps the most widely used methods in engineering practice for simulating FSI are based on arbitrary Lagrangian–Eulerian (ALE) formulations.[41,118] ALE methods for FSI problems are extensions of conventional finite element (FE) methods that treat the governing equations of conservation of momentum (Eqs. (1) and (2)), along with the coupling conditions (Eqs. (4) and (5)), using disjoint, dynami-

cally updated meshes for the fluid and structure regions. These methods enable the sharp resolution of velocities and stresses at fluid–structure interfaces, and facilitate the construction of graded meshes that can efficiently resolve fluid boundary layers. A substantial computational difficulty associated with ALE methods for FSI is the use of conforming geometrical descriptions of the fluid and structure grids, which necessitates frequent grid regeneration. It is also challenging to handle contact between solid bodies with ALE schemes. Despite these difficulties, ALE methods have found use both in experimentally-verifiable benchmark models[131] and in more realistic heart valve geometries.[28,30,117]

Two closely-related approaches to FSI that do not require the use of disjoint, geometrically-conforming descriptions of the fluid and structure regions are fictitious domain[57,168] and immersed boundary (IB)[126] methods, which both avoid the grid generation related difficulties of ALE schemes. In typical fictitious domain methods such as the method of distributed Lagrange multipliers (DLM),[57,168] distinct momentum equations are solved on both fluid and structure meshes. In the continuum equations, the velocity of the structure and fluid are required to match where these regions overlap; in the discrete equations, these matching conditions are approximately imposed by Lagrange multipliers that act as a forcing term in the momentum equations. Thus, in DLM methods, there is generally some relative slip between the fluid and structure, and this feature of the method seems to complicate simulations involving contact. By contrast, IB-type methods typically employ only a single momentum equation for both fluid and structure, and the no-slip condition is used directly to determine the motion of the immersed solid body. Consequently, all structures move according to a common continuous velocity field. This implies that disjoint structures cannot interpenetrate each other, at least in the semi-discrete case in which time is continuous. Thus, IB models of the heart valves readily handle contact between leaflets without using an auxiliary contact model.[58,62] The conventional limitations associated with fictitious domain and IB-type methods are that they yield relatively low accuracy at fluid–solid interfaces. Accordingly, well-resolved three-dimensional simulations require high spatial resolution that presently necessitates the use of high-performance computing resources. The IB method was introduced to model heart valves,[124,125] and both fictitious domain[37–40,147] and the IB methods[50,54,59–62,100,101,110,111,121,127] have been used substantially in modeling heart valve dynamics.

Immersed Boundary Methods for Elastic Structures

The IB formulation of the equations of motion (Eqs. (1) to (5)) adopts a Lagrangian description of the deformations and elastic stresses of the immersed solid along with an Eulerian description of the momentum, incompressibility, and viscous stresses of the coupled fluid–structure system.[126] Integral equations with Dirac delta function kernels couple the Lagrangian and Eulerian frames, and when the equations of motion are discretized for computer simulation, the singular delta function kernel is generally replaced by a suitable regularized delta function.[126] Assuming that the mass density of the fluid is equal to the mass density of the structure, so that $\rho^f = \rho^s = \rho$, and that the solid is viscoelastic with the same viscosity as the fluid, the equations of motion for the coupled fluid–structure system may be written as[18]

$$\rho \frac{D\boldsymbol{u}}{Dt}(\boldsymbol{x},t) = -\nabla p(\boldsymbol{x},t) + \mu \nabla^2 \boldsymbol{u}(\boldsymbol{x},t) + \boldsymbol{f}(\boldsymbol{x},t), \quad (15)$$

$$\nabla \cdot \boldsymbol{u}(\boldsymbol{x},t) = 0, \quad (16)$$

$$\begin{aligned} \boldsymbol{f}(\boldsymbol{x},t) = &\int_{\Omega_s^0} \nabla_{\boldsymbol{X}} \cdot \mathbb{P}(\boldsymbol{X},t)\, \delta(\boldsymbol{x} - \boldsymbol{\chi}(\boldsymbol{X},t))\, \mathrm{d}\boldsymbol{X} \\ &- \int_{\Gamma_s^0} \mathbb{P}(\boldsymbol{x},t)\, \boldsymbol{N}(\boldsymbol{X})\, \delta(\boldsymbol{x} - \boldsymbol{\chi}(\boldsymbol{X},t))\, \mathrm{d}A(\boldsymbol{X}), \end{aligned} \quad (17)$$

$$\frac{\partial \boldsymbol{\chi}}{\partial t}(\boldsymbol{X},t) = \int_{\Omega} \boldsymbol{u}(\boldsymbol{x},t)\, \delta(\boldsymbol{x} - \boldsymbol{\chi}(\boldsymbol{X},t))\, \mathrm{d}\boldsymbol{x}. \quad (18)$$

in which $\boldsymbol{f}(\boldsymbol{x},t)$ is the Eulerian elastic force density that accounts for the solid stresses, $\boldsymbol{N}(\boldsymbol{X})$ is the outward unit normal to Γ_s^0, and $\delta(\boldsymbol{x}) = \delta(x)\,\delta(y)\,\delta(z)$ is the three-dimensional delta function. Notice that the fundamental property of the Dirac delta function implies that

$$\frac{\partial \boldsymbol{\chi}}{\partial t}(\boldsymbol{X},t) = \boldsymbol{u}(\boldsymbol{\chi}(\boldsymbol{X},t),t). \quad (19)$$

Furthermore, for this IB formulation of the equations of motion, the solid stress $\boldsymbol{\sigma}^s$ is[51]

$$\begin{aligned} \boldsymbol{\sigma}^s(\boldsymbol{x},t) = &-p(\boldsymbol{x},t)\mathbb{I} + \frac{1}{J}\mathbb{P}\big(\boldsymbol{\chi}^{-1}(\boldsymbol{x},t),t\big)\mathbb{F}^T\big(\boldsymbol{\chi}^{-1}(\boldsymbol{x},t),t\big) \\ &+ \mu\big(\nabla \boldsymbol{u}(\boldsymbol{x},t) + \nabla \boldsymbol{u}^T(\boldsymbol{x},t)\big). \end{aligned} \quad (20)$$

With these assumptions on the form of $\boldsymbol{\sigma}^s(\boldsymbol{x},t)$ and the mass densities of the fluid and structure, this IB formulation can be shown to be equivalent to the more standard formulation described earlier on governing equations.[51] It is possible to extend this formulation to allow the density of the structure to be different from that of the fluid and to remove the viscosity of the immersed solid.[43,44,86,87,116,169] However, since heart valve leaflets are quite thin such extensions -the density differences- are not required to simulate heart valve dynamics. Accordingly, it is natural to use nonlinear

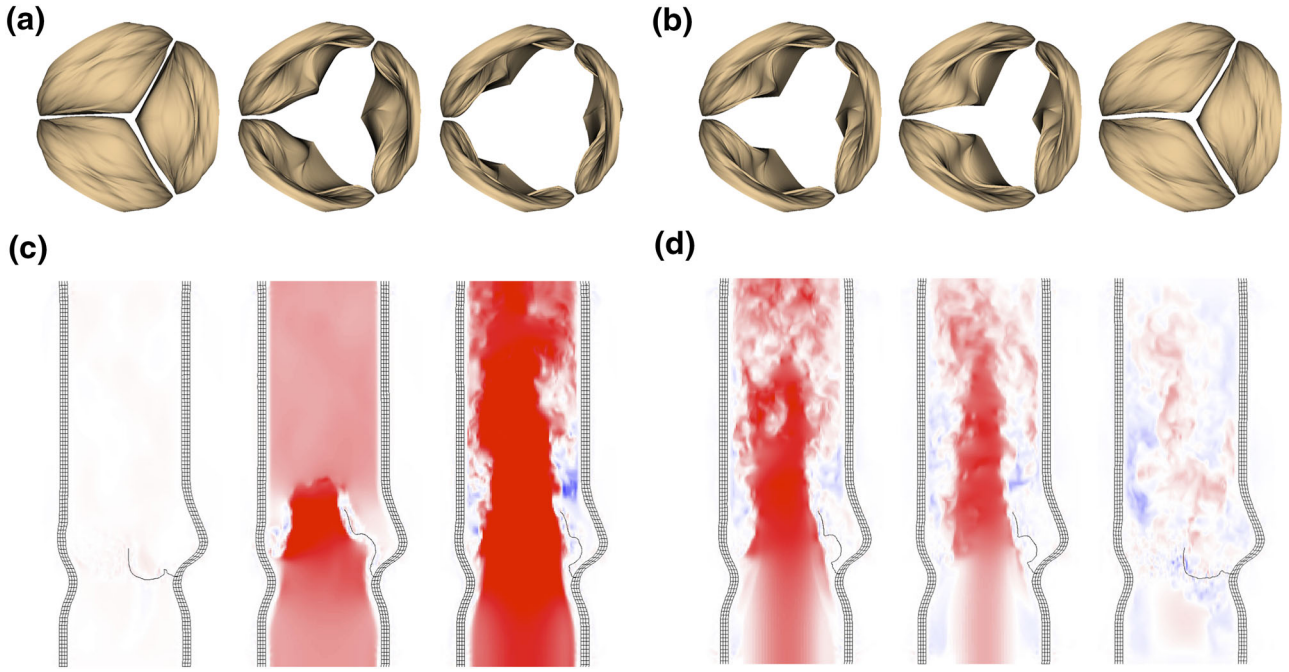

FIGURE 1. High-resolution immersed boundary/finite element model of the aortic valve. This model describes the flexible walls of the aortic sinuses and ascending aorta using an incompressible hyperelastic model fit to experimental tensile test data from human aortic sinus tissue samples[9] along with a fiber-reinforced model of the valve leaflets based on the mathematical theory of Peskin and McQueen.[128] Configurations of the valve leaflets are shown during valve opening (a) and closure (b), as viewed from the ascending aorta. The configurations of the aortic root model and axial flow patterns (*blue* −150 cm/s; *red* +150 cm/s) are shown at corresponding times during opening (c) and closure (d).

finite element (FE) methods[11,20] to discretize the Lagrangian equations.[18,51] Simulation results obtained using an IB/FE model of the aortic root are shown in Fig. 1.

Immersed Boundary Methods for Rigid Structures

The IB formulation of FSI problems involving immersed elastic bodies can be extended to treat rigid bodies such as mechanical heart valve leaflets. One approach, introduced by Peskin and Kim (unpublished), employs two different deformation mappings from reference coordinates to current coordinates, say $\boldsymbol{\chi}(\boldsymbol{X},t)$ and $\boldsymbol{\phi}(\boldsymbol{X},t)$. The dynamics of one of mappings are determined by the material velocity field $\boldsymbol{u}(\boldsymbol{x},t)$, so that

$$\frac{\partial \boldsymbol{\chi}}{\partial t}(\boldsymbol{X},t) = \boldsymbol{u}(\boldsymbol{\chi}(\boldsymbol{X},t),t), \tag{21}$$

whereas the dynamics of the other are required to be that of a rigid body, i.e.,

$$\frac{\partial \boldsymbol{\phi}}{\partial t}(\boldsymbol{X},t) = \boldsymbol{U}(t) + \boldsymbol{W}(t) \times \boldsymbol{X}. \tag{22}$$

A penalty force can then be introduced to approximately impose the constraint,

$$\boldsymbol{\chi}(\boldsymbol{X},t) = \boldsymbol{\phi}(\boldsymbol{X},t), \tag{23}$$

which implies that the immersed body moves as a rigid body. The resulting equations of motion are

$$\rho \frac{D\boldsymbol{u}}{Dt} = -\nabla p(\boldsymbol{x},t) + \mu \nabla^2 \boldsymbol{u}(\boldsymbol{x},t) + \boldsymbol{f}(\boldsymbol{x},t), \tag{24}$$

$$\nabla \cdot \boldsymbol{u}(\boldsymbol{x},t) = 0, \tag{25}$$

$$\boldsymbol{f}(\boldsymbol{x},t) = \int_{\Omega_s^0} \mathbf{F}(\boldsymbol{X},t)\, \delta(\boldsymbol{x} - \boldsymbol{\chi}(\boldsymbol{X},t))\, \mathrm{d}\boldsymbol{X}, \tag{26}$$

$$\frac{\partial \boldsymbol{\chi}}{\partial t}(\boldsymbol{X},t) = \int_{\Omega} \boldsymbol{u}(\boldsymbol{x},t)\, \delta(\boldsymbol{x} - \boldsymbol{\chi}(\boldsymbol{X},t))\mathrm{d}\boldsymbol{x}, \tag{27}$$

$$\frac{\partial \boldsymbol{\phi}}{\partial t}(\boldsymbol{X},t) = \boldsymbol{U}(t) + \boldsymbol{W}(t) \times \boldsymbol{X}, \tag{28}$$

$$\boldsymbol{F}(\boldsymbol{X},t) = \kappa(\boldsymbol{\phi}(\boldsymbol{X},t) - \boldsymbol{\chi}(\boldsymbol{X},t)), \tag{29}$$

in which κ is a penalty parameter and $\boldsymbol{F}(\boldsymbol{X},t)$ is the (Lagrangian) penalty force that approximately imposes the rigidity constraint. In the limit of $\kappa \to \infty$, $\|\boldsymbol{\chi}(\boldsymbol{X},t) - \boldsymbol{\phi}(\boldsymbol{X},t)\| \to 0$ and the rigidity constraint are imposed exactly.

If the mass density of the rigid body is greater than that of the fluid, the dynamics of $\boldsymbol{U}(t)$ and $\boldsymbol{W}(t)$ are determined from the requirement that the rate of change of the "excess" linear and angular momentum is proportional to the net force and torque acting on the body, i.e.,

$$\frac{d\boldsymbol{P}}{dt}(t) = -\int_{\Omega_s^0} \boldsymbol{F}(\boldsymbol{X},t)\,\mathrm{d}\boldsymbol{X}, \tag{30}$$

$$\frac{d\boldsymbol{L}}{dt}(t) = -\int_{\Omega_s^0} \boldsymbol{F}(\boldsymbol{X},t)\times\boldsymbol{X}\,\mathrm{d}\boldsymbol{X}, \tag{31}$$

in which the excess linear and angular momentum are, respectively

$$\boldsymbol{P}(t) = \tilde{\rho}\boldsymbol{U}(t), \tag{32}$$

$$\boldsymbol{L}(t) = \mathbb{I}_{\tilde{\rho}}\boldsymbol{W}(t), \tag{33}$$

where $\tilde{\rho} = \rho^s - \rho^f$ is the excess mass density of the solid and $\mathbb{I}_{\tilde{\rho}}$ is the corresponding moment of inertia tensor. For a neutrally buoyant body, $\tilde{\rho} = 0$ and $\boldsymbol{U}(t)$ and $\boldsymbol{W}(t)$ are determined directly from the requirement that there should be no net force or torque on the immersed rigid body. Simulation results obtained using this IB/FE formulation for immersed rigid bodies are shown in Fig. 2 for a model of a mechanical prosthetic valve.

Validation

There is a clear need for the systematic verification and validation of FSI models of native and prosthetic heart valves, both in comparison to benchmark experimental data and also to clinical imaging data. Substantial challenges still remain. As part of its *Critical Path Initiative*, the U.S. Food and Drug Administration (FDA) has been working to determine the role of computational fluid dynamics (CFD) in regulation of the cardiac devices. An initial FDA study compared CFD predictions of flow through an idealized cardiovascular device to experimental particle image velocimetry (PIV) data of flow through the same device.[145,146] Numerical results from 28 independent computational groups were compared to data acquired by three experimental laboratories. The experimental data were in good agreement, but substantial discrepancies existed among the numerically predicted velocities and shear stresses in comparison to the experimental data. Furthermore, large discrepancies were observed between the predictions of different numerical models. Accurate modeling of the shear stress is especially important for predicting device safety because shear stress is used as a proxy for blood damage (hemolysis) and, in more complex models, "triggers" the accumulation of damage.

Currently, FSI valve models have been validated almost exclusively by comparison to *in vitro* experimental data,[30,35,52,53,131,147] and in most of these cases, the model corresponds to a mechanical valve rather than a flexible native or bioprosthetic valve. Furthermore, these comparisons to experimental data focus on the opening and forward-flow phases, and generally do not consider valve closure. Direct comparisons of valve models to clinical data are largely unreported in the literature. There appear to be relatively few FSI valve models that can perform multiple cardiac cycles and also simulate the closed, loaded configuration of the valve,[49,58,62] presumably due to the computational challenges associated with simulating contact between thin flexible structures under realistic transvalvular pressure loads. Such models also have not yet been subjected to substantial validation for valve closure's mechanism. Closure seems to be especially challenging to simulate because it fundamentally involves a delicate balance between the fluid dynamics and elasticity of the valve's leaflets. Obtaining fully resolved simulations of valve closure seem to require higher-resolution simulations than that of presently feasible, and we

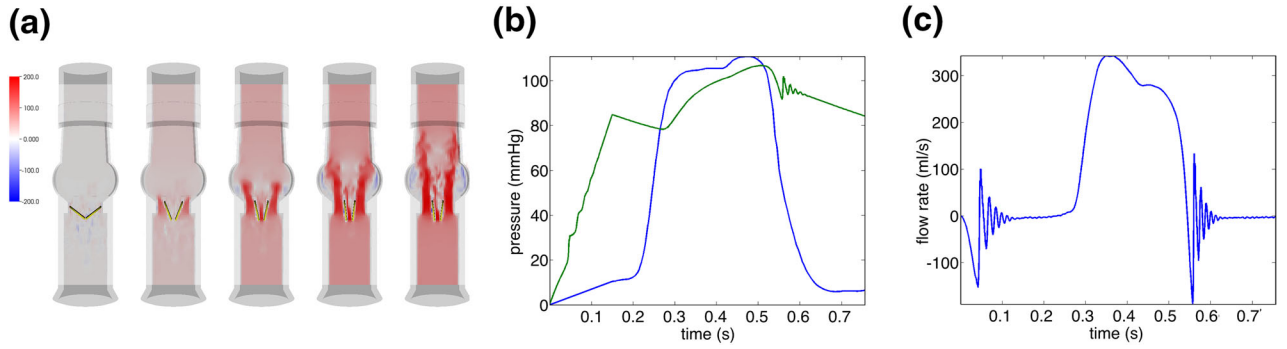

FIGURE 2. Simulation results obtained using a three-dimensional FSI model of a mechanical aortic valve prostheses mounted in a commercial pulse duplicator (Vivitro Systems, Inc.) using an IB/FE approach to modeling rigid bodies.[60] (a) Opening dynamics (b) prescribed driving pressure (blue) and computed loading pressure (green), and (c) computed flow rate.

anticipate that such simulations will motivate the development of improved numerical methods for FSI.

MULTISCALE MODELING

In recent years, major efforts have been made towards creating functional models of the heart valves that relate different scales to each other's.[29,144,160] Given the multiscale nature of the valve biomechanics, linking the organ scale to tissue and cell scales and ultimately to molecular scales, should lead to a full understanding of the disease mechanisms and processes. This would necessitate multiscale models that can seamlessly span and link these disparate scales (see Fig. 3).[160]

With recent advances in computational technologies, it is becoming increasingly possible to develop patient-specific models that can be used for better design and evaluation of surgical interventions as well as prediction of progression of heart valve disease and catastrophic failure of the prosthetic valves. This necessitates incorporating geometrical, structural and mechanochemical attributes of the disease. As a first step in this direction, multiscale models of the bicuspid and tricuspid aortic valves with regards to calcific aortic stenosis have been developed (see Fig. 4).[161] While the aortic valve is naturally comprised of three cusps and their surrounding tissue, some patients are born with a bicuspid aortic valve. It is well known that these patients are more likely to develop a calcific aortic stenosis than their cohorts with normal tricuspid aortic valves.[167] In a healthy heart valve, each cusp is thin and pliable while in calcific aortic stenosis, the calcified nodules develop and spread across the cusps. It is currently not known whether the risk increase in calcific aortic stenosis is due to the geometric differences between the tricuspid and bicuspid valves or whether it is because of the same underlying genetic conditions that produce the geometric difference. Weinberg *et al.* employed multiscale models of the aortic valve and isolated the effect of one geometric factor, namely the number of cusps, to explore its effect on multiscale valve mechanics, with regards to calcific aortic stenosis.[161] The bileaflet and trileaflet aortic valves were modeled by a set of simulations describing the cell, tissue, and organ length scales. These models were linked across the length scales to create a coherent multiscale model. At each scale, the models are three-dimensional and dynamic, incorporating accurate nonlinear constitutive models of the valve leaflet tissue. Results were compared between the two valve types at each length scale. At the cellular scale, the region of interest was the location where calcification develops, near the aortic-facing surface of the leaflet. The simulations showed the expected differences between the tricuspid and bicuspid valves at the organ scale: the bicuspid valve shows greater flexure in the solid phase and stronger jet formation in the fluid phase compared to the tricuspid valve. However,

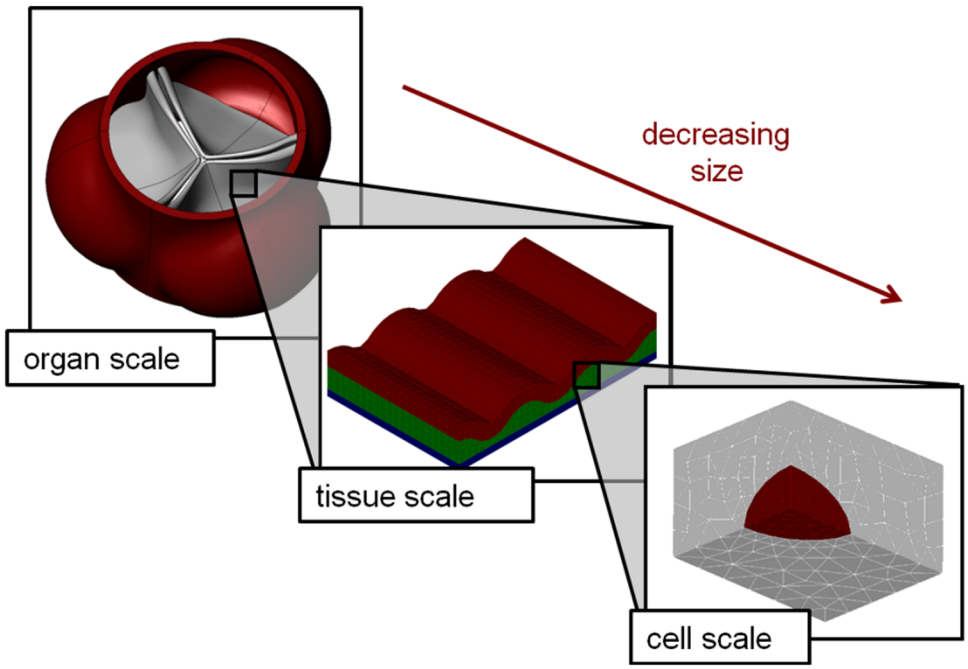

FIGURE 3. Schematic of a multiscale model of the aortic valve, linking the organ, tissue and cellular scales. Deformations are mapped from largest scale to smallest (taken with permission from Weinberg and Mofrad[161]).

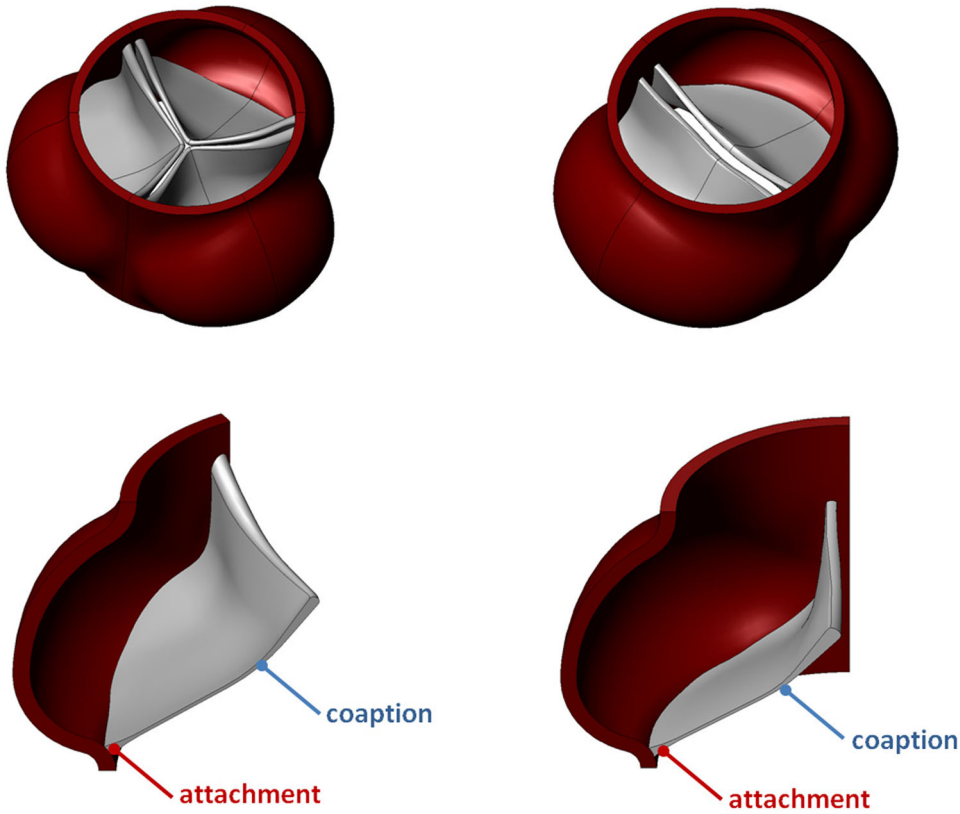

FIGURE 4. Organ-scale valve geometries, tricuspid on left and bicuspid on right. Top: full geometry of valve. Bottom: cutaways showing tracking locations (adapted with permission from Weinberg *et al.*[162]).

at the cellular scale, the models suggested that the region of interest may be shielded against strain by the wrinkling of the fibrosa layer.[112] Thus, the cellular deformations were not significantly different between the bileaflet and trileaflet aortic valves in regards to the calcification-prone regions. These results suggested that the difference in calcification observed in the bileaflet vs. trileaflet aortic valve may be primarily due to the factors other than the simple valve's geometry.[161]

In calcific aortic stenosis calcified nodules progressively stiffen the cusps. The local mechanical changes in the cusps, due to either normal aging or pathological processes, affect the overall valve function. Weinberg *et al*. developed a computational model for the aging aortic valve that connects local changes to overall valve function.[162] In this model, the aging and calcification processes were simulated by varying the thickness and extensibility of the leaflets (see Fig. 5). This simulation was the first analytical tool to describe the temporal behavior of aortic valve calcification.

DISEASE SPECIFIC MODELING

A combination of computational and experimental studies is needed to capture the underlying mechanisms of heart valve disease. It has been shown that the hemodynamic environments from opposing sides of the human aortic valve leaflets evoke distinct endothelial phenotypes *in vitro*.[158] While the cellular and molecular mechanisms leading to valvular pathogenesis remain unknown, the effect that the hemodynamic environment imposes on valvular endothelial cells, as well as the valve structure and function, has gained recent attention. The researchers described the specific shear waveforms to which the two sides of the aortic valve cusp are subjected to, and thus recreated the specific hemodynamic environment of the valve surfaces *in vitro*. The shear waveforms applied by the blood flow to the aortic and ventricular sides of the valve endothelium were extracted from computational models and applied to cultured human endothelial cells in order to investigate whether these waveforms influence endothelial gene expression. Using this *in vitro* model, the cells exposed to the ventricular waveform were found to display an anti-inflammatory endothelial molecular phenotype, compared to cells exposed to the waveform from the aortic side of the leaflet.

An emerging area in computational and theoretical modeling of the heart valve involves the simulation of active mechanochemical processes underlying the valvular disease. Detailed understanding and predic-

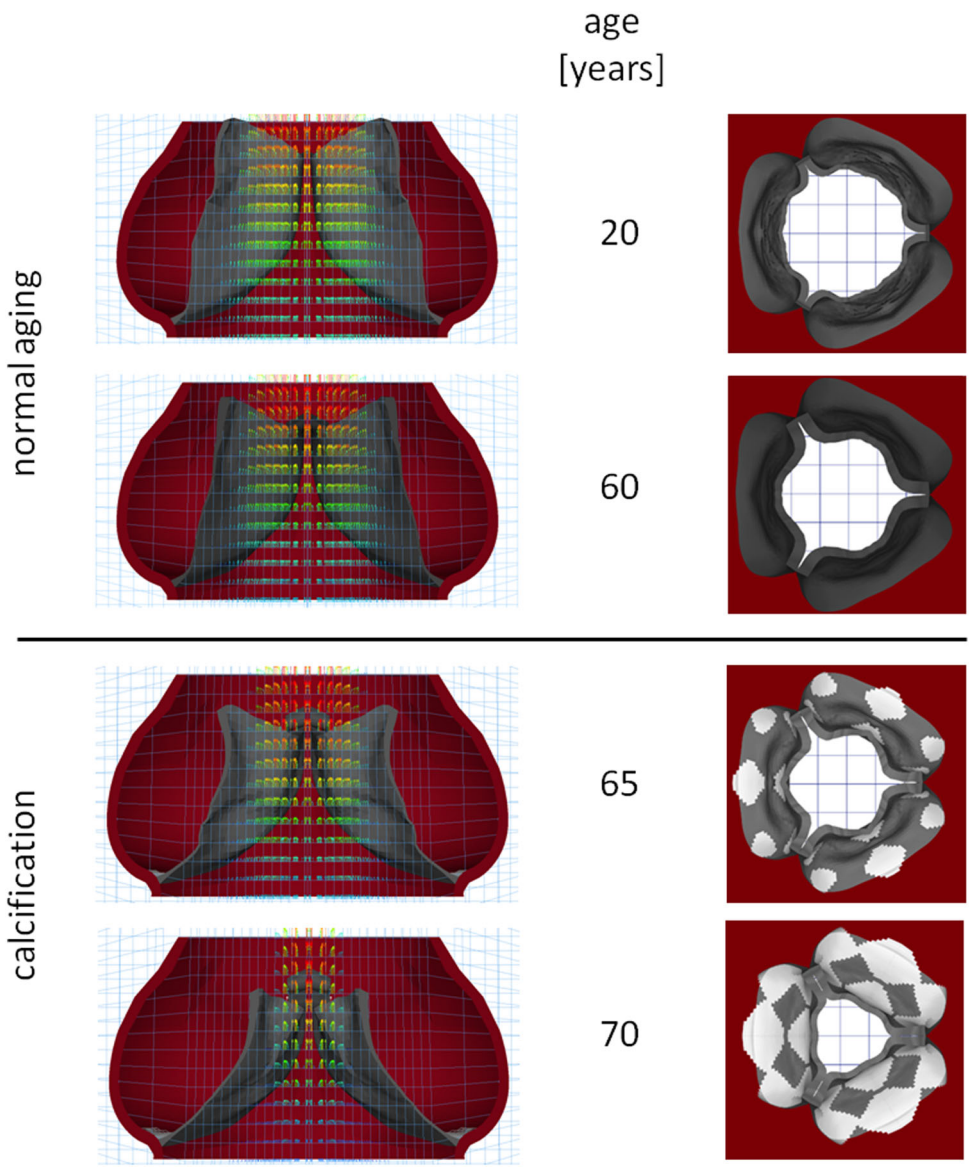

FIGURE 5. A computational/analytical model to describe the temporal behavior of aortic valve calcification. Computed geometries and flow velocities are shown at mid-systole at various ages. Assumptions for calcification model are onset at age 50 and a growth rate of 1 mm/year Weinberg *et al.*[162].

tion of the diseases mechanisms requires a detailed appreciation of the molecular pathways that link the leaflet tissue mechanics to the signaling networks. These networks carry the extracellular signals to the participating cells and their nuclei to elicit the biological response that ultimately yields the initiation and progression of a disease. To understand valvular disease, we need to understand the mechanisms through which external factors/signals influence the biological response of the valvular cells and their consequent mechanotransduction signals that are transduced to the underlying proteins.[71,113] These in turn lead to conformational changes in individual proteins that elicit biological responses reflected in the valve disease. Computational methods are essential that range from large-scale, whole valve models down to molecular dynamics models of proteins. Such models are needed as the mysteries of valvular disease are unraveled.

EXPERIMENTAL EFFORTS

In vitro Calcification Assessment

Structural degradation and dysfunction is the predominant cause of failure of tissue-based heart valves. Glutaraldehyde fixation of the leaflets, which is a required process in manufacturing bioprosthetic valves, has been shown as a mechanistic factor

responsible for bioprosthetic cuspal calcification.[2,93] The dystrophic hydroxyapatite deposition is mainly initiated by the devitalized, residual cellular matter in the pericardial leaflets. Plasma membrane-associated phosphorus interacts with the calcium in the extracellular fluid, causing calcium phosphate to be deposited on the tissue.[152] Following calcification, secondary tears, cuspal stiffening, and pure stenosis may also occur, leading to valve failure.

Presence of valvular calcification in a patient is one of the most predictable factors that lead to the device failure. However, as mentioned earlier, predicting the factors that promote calcification is difficult.[140] Calcification assays *in vitro* can be performed using static and dynamic testers to study the factors that promote heart valve calcification.[12,56,155,165] Dynamic *in vitro* testers are particularly useful in studying the process of calcification in bioprosthetic heart valves.[12] A dynamic testing apparatus consists of a fatigue tester or other oscillating chamber filled with a calcifying solution that contains a range of different simple salt solutions with physiological and supra-physiological concentrations of calcium and phosphate.[65,75,89,141] Depletion of calcium and phosphate as well as calcium uptake by the valves' leaflets can be used to determine the rate and progression of passive calcification.[12] This uptake can be determined chemically or by imaging the tissue density. In addition to passive calcium/phosphate uptake experiments, the effects of surface defects such as roughness and cracks, and low and high flow shear rate on the calcification process of the bioprosthetic heart valves can be studied.[19]

Imaging modalities such as X-ray and micro-CT have been used to quantify the degree of calcification of the experimentally treated tissues. Furthermore, more recent studies have used Inductively Coupled Plasma spectrometry and EDX (Energy Dispersive X-ray) spectroscopy for quantification of calcification.[19] An example of this type of testing is monitoring the effects of polydimethylsiloxane (PDMS) on calcification *in vitro*.[32,78,104,105] Scanning electron microscopy (SEM) and X-ray absorption near edge structure (XANES) were also used to investigate calcified native and bioprosthetic heart valves and to characterize morphology and chemical composition.[163]

While *in vitro* calcification studies have been performed to test passive calcification deposition of the heart valves, it should be noted that these studies do not necessarily rule out the potential active calcification of the heart valves *in vivo*.[12,102,129,139,141]

Accelerated Wear Testing

Improper design features in prosthetic heart valves may result in dysfunction and even to catastrophic failure.[67] The harsh physiologic environment inside the heart along with the fact that a heart valve undergoes millions of opening and closing cycles requires careful *in vitro* testing to ensure the longevity of the implant. These tests must ensure that fatigue fracture and wear do not adversely harm the implant. During its lifespan, a bioprosthetic heart valve undergoes flexure of the valve cusps. This combines with cyclic compressive and tensile stresses,[153,154] may result in tissue failure due to fiber disruption.[149] High pressure fixation of first generation of bioprosthetic valves in glutaraldehyde enhanced the durability of these valves but resulted in early calcification.[23,48,72,74] The second generation of heart valves treated by zero to low pressure fixation (e.g., the Hancock II porcine valve, Medtronic, Inc, Minneapolis, MN, and the Carpentier-Edwards Perimount^{TM}, Edwards Lifesciences, Irvine, CA), have been implanted in patients for more than two decades with minimal problem.[27,36,109] Alternatively, third generation of heart valves such as Carpentier-Edwards Magna model of the Perimount^{TM} pericardial prosthesis (Edwards Lifesciences, Irvine, CA) and the Mosaic porcine valve (Medtronic, Inc., Minneapolis, MN) have only been implanted for approximately 13 years.[34,73,133,134], making it too early to determine their durability compared to older generations.[31]

The loading conditions that a prosthetic heart valve is exposed to are very complicated and cannot be fully replicated by simple fatigue testing. For example, in transcatheter heart valves, loading conditions not only include leaflet bending, torsion, radial dilatation and compression, but also it requires testing the linear/transverse compression of the stent, its axial tension and compression. These parameters can also be significantly diverse for different valves. Therefore, *in vitro* testing must be validated in terms of applying the loads and deformations that a particular device will experience. To examine the structural reliability of heart valves, they undergo 400 or 600 M cycles which meet or exceed the cycles that the valve experience after implantation.[79] Table 1 shows the minimum cycles needed for testing as requited by regulatory agencies.

Regulations for approval of medical devices in the United States are governed by the Food and Drug Administration (FDA). For cardiac valve prostheses the FDA relies upon recommendations set forth by the International Organization for Standardization (ISO). The ISO's 5840, parts 1-3, outline the requirements for surgically implanted heart valve substitutes and heart valves implanted by transcatheter techniques. These requirements include hydrodynamic testing, durability testing and flow visualization. Hydrodynamic testing and flow visualization are performed to provide information on the fluid mechanical performance of the heart valve substitute and provide indicators of

valve performance in terms of load to the heart and potential for blood stasis and damage. Hydrodynamic testing can be accomplished by using pulsatile flow, steady back-flow leakage testing and steady forward flow testing. Durability testing is typically completed using a robust high frequency durability tester (Fig. 6). Finally, flow visualization can be accomplished by many imaging modalities, with particle image velocimetry (PIV) being a popular example.[45,66,81] By incorporating PIV, investigators can use pulsatile flows and quantify with a high degree of accuracy fluid dynamics such as shear stresses and turbulent shear stresses.[45] This allows for a quantitative assessment of the hemolytic and thrombogenic potential of the valve design in each position of intended use.[66,82]

IN VITRO CORROSION TESTING

Similar to other implantable devices, heart valves are also subjected to corrosion, particularly the transcatheter heart valves that are enclosed by a metal stent. Degradation of the heart valve due to a reaction with its environment may cause catastrophic damage. It is therefore important to optimize the surface to ensure conditions that prevent degradation. Stented valves can be tested by electrochemical corrosion testing and advanced surface analysis. In addition, Auger Electron Spectroscopy (AES) can measure the surface oxide layer thickness, and *in vitro* testing can be beneficial for detecting corrosion byproducts. A promising corrosion test should be carefully designed to characterize the mechanism of corrosion as well as the interactions between the material properties, surface finish, manufacturing, device design, and operational conditions. ASTM F2129, ASTM F746 are among the commonly used methods for corrosion testing of medical devices. Furthermore, electrochemical impedance spectroscopy and electrochemical noise measurements can track corrosion during accelerated testing.[79] As required by FDA, the corrosion resistance of the material in a heart valve should be determined in a physiological environment and under stress before and after fatigue testing.

HYDRODYNAMIC ASSESSMENT OF HEART VALVES

Hydrodynamic testing of the heart valves is an important step for preclinical studies of a new device. Transvalvular pressure gradients, Reynolds stresses, particle residence time and shear stress that a heart valve generates have been identified performance indicators for these devices. Several complex experimental setups have been described in the literature that

TABLE 1. Minimum *in vitro* fatigue testing cycles required for prosthetic heart valves.[79]

	Bioprosthetic valve	Mechanical valve	Structural component
ISO 5840	200 M (5 years)	400 M (10 years)	400 M (10 years)
US FDA	200 M (5 years)	600 M (15 years)	600 M (15 years)

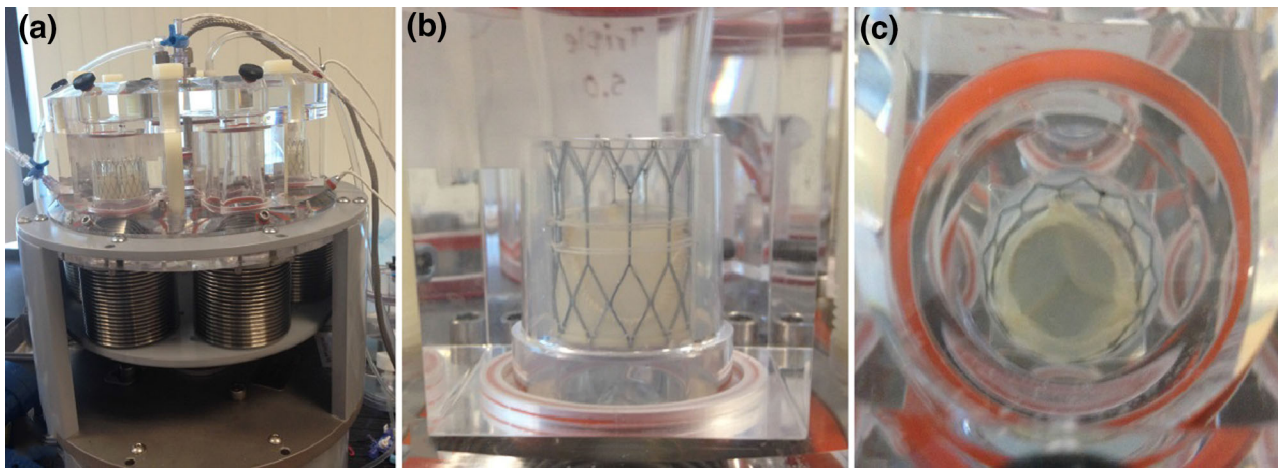

FIGURE 6. Accelerated durability testing. (a) Dynatek Labs M6 tester designed specifically for heart valves. (b) An example of a transcatheter heart valve (FoldaValve, FOLDA, LLC, Rancho Santa Margarita, CA) positioned inside its custom-designed chamber of the durability tester. (c) FoldaValve[80] transcatheter heart valve under accelerated durability testing, top view. Images are from Kheradvar Laboratory.

was used for hydrodynamic tests. The first velocity recordings for transmitral flow were performed by Bellhouse and Bellhouse to study valve closure *in vitro*.[10] They built a transparent model of left ventricle with a mitral valve and connected that to a pulsatile pump to simulate transmitral flow. Kheradvar *et al.* experimentally studied the effect of the profile height of the mitral bioprosthetic valves on transmitral flow in a heart flow simulator, which comprised of a silicone ventricle, shaped according to molds in systolic state of the left ventricle that was immersed in a closed Plexiglas water tank connected to a pulsatile pump.[82] A comparable setup was also used to quantify the mitral annulus dynamics and its association to transmitral vortex formation during rapid filling.[83] Another study by Pierrakos *et al.* compared the effect of heart valve implantation orientations (i.e., anatomical and anti-anatomical positions) using experimental fluid dynamics.[130] In that study, a piston-driven left ventricular simulator capable of adjusting the heartbeat and the volume flow rate was used. More recent systems have been described by Arjunon *et al.*[8] and Linde *et al.*[99]

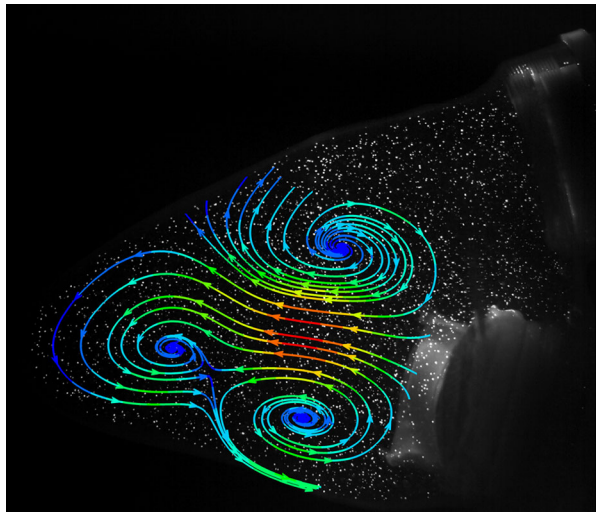

FIGURE 7. Flow streamline downstream of a bileaflet mitral bioprosthesis[81] resulting from the velocity vector field obtained by DPIV. Vortices formed around the transmitral jet were visualized by high speed digital particle image velocimetry in a heart flow simulator.[45] Neutrally buoyant, orange fluorescent particles with the diameter in the range of 60–80 μm were used for seeding the flow. Streamlines are shown in mid diastole and are colored by velocity magnitude. Image is from Kheradvar Laboratory.

PARTICLE IMAGE VELOCIMETRY OF HEART VALVES

Qualitative visualization of physiological flows by using tracer particles has been in practice for many years[95] and was originated in the drawings of Leonardo da Vinci.[92] Hot wire anemometry and laser Doppler velocimetry were used for quantitative *in vitro* flow studies. However, these methods were only capable of providing point-wise information. Image processing of the flow downstream of the heart valves was first introduced in late 1980s[1] and provided useful velocity field information.[1,33,96] After introduction of digital particle image velocimetry (DPIV),[164] the techniques ability to provide quantitative velocity information in vicinity of the prosthetic heart valves started a new era of flow analysis.[142] In 2004, Grigioni *et al.*[63] summarized laser techniques employed for the investigation of the fluid dynamics of artificial heart valves.

DPIV in its various forms such as time-resolved PIV and high speed DPIV (that does not require averaging the flow over multiple cycles) substantially improved our understanding from the flow past through the prosthetic heart valves (Fig. 7).[17,26,45–47,64,66,68,76,77,88,91,97,98,103,130,138] However, PIV methods were mainly two dimensional until Brücker introduced Stereo-PIV based on the use of two digital cameras and PIV algorithms to study the flow past artificial heart valves.[21] The testing requirements for performing stereo-PIV for characterizing the flow through mechanical heart valves has been well described by Morbiducci *et al.*[115]

Another breakthrough in PIV was the development of defocusing digital particle image velocimetry (D-DPIV).[123] In D-DPIV, particle depth information is defined by quantifying the natural blurring of the particles as they move out of the focal plane. The D-DPIV technique uses three cameras and identifies the image shift produced by the apertures to measure the depth of the particle from each camera. D-DPIV has also been used to visualize the flow through artificial heart valves.[6] In that work, Amatya *et al.* identified 3D instantaneous and ensemble-averaged flow features around a mechanical and a silicone polymer valve.[6] More recently, multiplanar PIV (MPPIV) has been introduced to measure the flow in three dimensions.[46] This method uses two-dimensional, two-component velocity fields acquired on multiple perpendicular planes and reconstruct them into a 3D velocity field through Kriging interpolation and imposing the incompressibility constraint.[46]

COLLAGEN FIBER ORIENTATION AND COMPUTATIONAL MODELING

Accurate computational modeling of a heart valve requires incorporating important structural features such as how its collagen fibers are concentrated and aligned in the leaflets (Fig. 8). Different collagen fiber directions affect the mechanical response of the

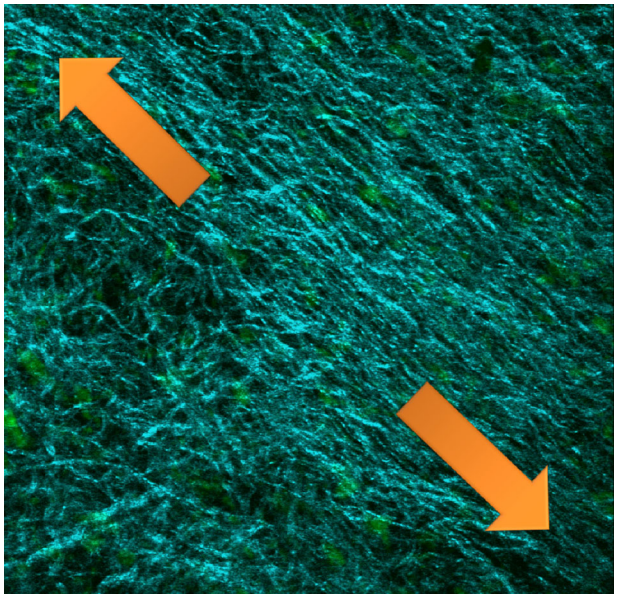

FIGURE 8. The architecture of the collagen fibers in the leaflet of a porcine mitral valve. The second harmonic generation microscopy shows the arrangement of collagen fibers in their relaxed state. The image was taken at 60 microns depth from the surface at belly of the leaflet. Image is from Kheradvar Laboratory.

tissue,[3,15,114] making it important to consider in computer simulations of a heart valve.[24,37,135,156] Early modeling of fiber efforts were performed by Peskin and McQueen who generated an array of fibers that functioned as an aortic valve.[128] Later studies used finite element analysis to study mechanically induced collagen fiber remodeling in the aortic heart valve.[42]

In order to accurately model the dynamics and kinematics of a valve leaflet, collagen fiber orientation should be precisely considered in the model. Alavi *et al.* used advanced imaging tools such as Second-Harmonic Generation (SHG) microscopy to characterize the 3D collagen fiber arrangement of native valve leaflets and bovine pericardial tissue leaflets in response to a variety of different loading conditions.[3] They showed that the collagen fibers do not necessarily all align with the load in each layer throughout the depth of tissue. This insight improved our understanding of the pathophysiology of native valves in response to stress and can be used to develop more accurate constitutive and computational models of the heart valves.

Sun *et al.* modeled the quasi-static leaflet deformation of a bioprosthetic heart valve under quasi-static transvalvular pressures according to a Fung-elastic material model that incorporates the leaflet collagen fiber structure.[148] Kheradvar and Falahatpisheh[81] modeled a bileaflet mitral bioprosthesis according to a constitutive model by May-Newman and Yin[108] that takes into account the leaflet's fiber direction:

$$W(I_1, I_4) = \overline{c_0}\left[\exp\left(\overline{c_1}(I_1 - 3)^2 + \overline{c_2}\left(\sqrt{I_4} - 1\right)^4\right) - 1\right] \tag{34}$$

where W is the strain-energy function, and $c_i (i = 0, 1, 2)$ are the independent material constants that characterize the deviatoric deformation of the leaflet material.[159]

MATERIAL MODELS AND BIAXIAL STUDIES

For several billion cardiac cycles, mitral and aortic valves –in contrary to tricuspid and pulmonary valves- should stand the high-pressure environment inside the left ventricle, and by design, possess high mechanical durability. Understanding the mechanical properties of heart valves is necessary to study valvular behavior and to design better prosthetic heart valves. Likewise, studying the leaflets' stress distributions can provide insight into mechanisms for pathological structural remodeling such as fibrosis and calcification. Considering that the stress cannot be directly measured in a heart valve, computational methods such as finite element analysis are needed to estimate it. To accomplish this, it is necessary to know the tissue microstructure, material behavior, loading conditions, and *in vivo* deformation. Material behavior of the leaflets is among the most important components required for estimation of the stress distribution. Using experimental setups to determine the tissue behavior and accordingly relate stress to deformation or strain is critical. Tensile testing has been extensively used to characterize the mechanics of the tissue. Uniaxial tension test was used to mechanically examine porcine mitral valve leaflets that showed the mitral valve tissue is a fiber reinforced composite and its stiffness is related to density and the direction of its fibers.[90] The relation between stress and strain for mitral valve leaflets has proven to be nonlinear, and the modulus of the leaflet adjacent to the chordae tendineae is 4–5 times greater than the center of the cusp. This was found based on examination of the uniaxial stress/strain characteristics of the mitral valve leaflets.[55] The locations of these regions are shown in Fig. 9. More recently, Alavi *et al.* characterized the extracellular matrix organization of the atrioventricular (AV) valves in both stress-free and loaded conditions.[4] They found that in the stress-free state, the collagen distribution is significantly different in mitral and tricuspid valves. Furthermore, under the uniaxial loading condition, the fibers rearranged differently in each valve type, to a configuration according to their previous relaxed states.[4] According

to the same study, the biaxial response of the AV valves was quite similar and found independent of their relaxed configuration.

While uniaxial loading provides an insight to tissue leaflets behavior, it does not provide sufficient information for the material behavior of these anisotropic tissues. This is mainly due to the heterogeneity in the tissue microstructure that leads to anisotropic behavior. Humphrey and Yin developed a pseudostrain-energy function for the constitutive relations of passive cardiac tissue when the deformations are finite,[70] which can be fitted to the data obtained from biaxial testing. They assumed a pseudostrain-energy function, $W(\mathbb{C})$, which in the following form can be written for both non-interacting densely distributed thin hyperelastic fibers and for homogeneous matrix:

$$W = W_m(\mathbb{C}) + \mathbb{W}_{\mathrm{f}}(\alpha) \tag{35}$$

where W_m and W_f are the energy stored in the matrix and the fibers, respectively. $\mathbb{C} = \mathbb{F}^T \cdot \mathbb{F}$, is the right Cauchy-Green deformation tensor, and $\mathbb{F}$ is the deformation gradient tensor. It was also assumed that W_f depends on $\mathbb{C}$ only through a fiber stretch ratio, α:

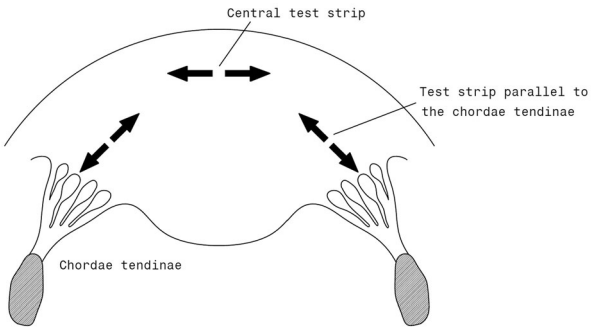

FIGURE 9. Locations of the test strips of the mitral valve leaflet sample[55]: close to chordae tendinae and the center of the cusp. The figure is adapted from Ghista and Rao.[55]

$$\alpha^2 = \mathbf{N} \cdot \mathbb{C} \cdot \mathbf{N} \tag{36}$$

Considering the strain energy function, the general constitutive relation of the tissue in loading and unloading can be described as:

$$\boldsymbol{\sigma} = -p\mathbb{I} + 2\mathbb{F} \cdot (\partial \mathbb{W}/\partial \mathbb{C}) \cdot \mathbb{F}^{\mathbb{T}} \tag{37}$$

Green's strain, $\mathbb{E}$, is computed from the deformation gradient tensor $\mathbb{F}$:

$$\mathbb{E} = \frac{1}{2}\left(\mathbb{F}^T\mathbb{F} - \mathbb{I}\right) \tag{38}$$

Cauchy stress $\boldsymbol{\sigma}$ is calculated from the first Piola-Kirchoff stress $\mathbb{P}$,

$$\boldsymbol{\sigma} = \frac{1}{J}\mathbb{P}\mathbb{F}^{\mathbb{T}} \tag{39}$$

May-Newman and Yin[108] formulated a strain energy function according to the fibrous architecture of the mitral valve, which describes large deformation and nonlinear transversely isotropic behavior. Billiar and Sacks[13,15] were the first to develop a constitutive model for the aortic valve using a specialized biaxial testing method designed for aortic valve cusp (Fig. 10)[136,137]:

$$\begin{cases} E_{CC} = \frac{1}{2}\left(\Lambda_C^2 - 1\right) = \frac{1}{2}\left(\lambda_C^2 + \kappa_R^2 - 1\right) \\ E_{RR} = \frac{1}{2}\left(\Lambda_R^2 - 1\right) = \frac{1}{2}\left(\lambda_R^2 + \kappa_C^2 - 1\right) \\ E_{CR} = E_{RC} = \frac{1}{2}\left(\lambda_C\kappa_C + \lambda_R\kappa_R\right) \\ \alpha = \sin^{-1}\left(\frac{2E_{CR}}{\sqrt{1+2E_{CC}}\sqrt{1+2E_{RR}}}\right) \end{cases} \tag{40}$$

Here E_{CC}, E_{RR}, and E_{CR} are in-plane Green's strain components; $_C$ and $_R$ are stretch ratios in the circumferential and radial directions; α is the shear angle. Using biaxial testing, it was shown that the circumferential elastic modulus of a porcine aortic valve

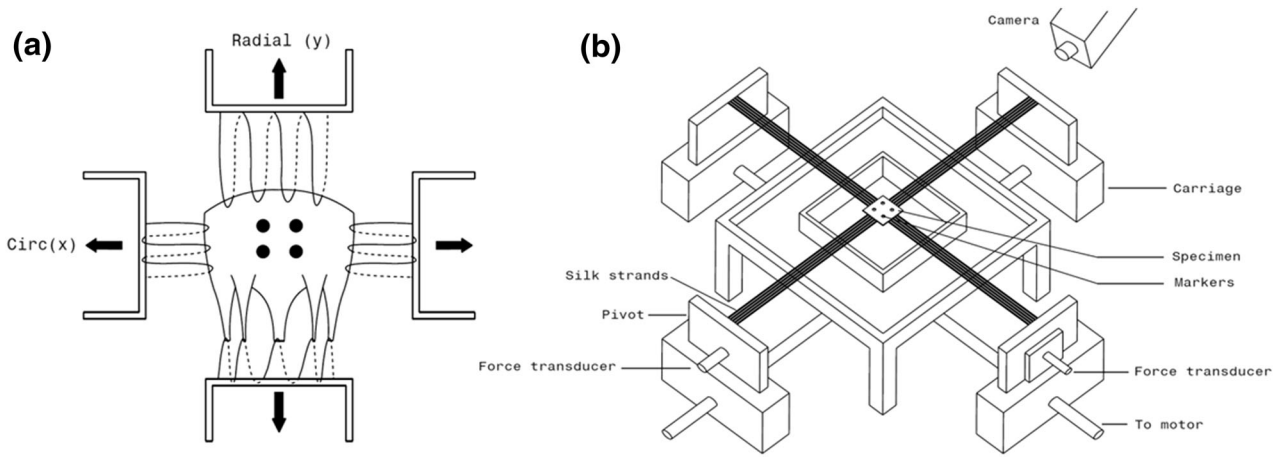

FIGURE 10. The schematic figure of the biaxial tester used by May-Newman and Yin.[107]

leaflet is much larger than the radial elastic modulus due to the fact that the fibers alignment is mainly in the circumferential direction.[13,16] Li *et al.*[94] developed another nonlinear anisotropic model for porcine aortic heart valves based on uniaxial experimental data and the properties of nonlinear composite. They showed that the anisotropic characteristics of the leaflet lead to significant changes in stress distribution. The location of the peak stress in an anisotropic leaflet was found to be different compared to an isotropic leaflet. Likewise, Bischoff *et al.*[16] developed a strain energy function based on the entropy change related to the deformation of constituent macromolecules to predict nonlinear orthotropic elastic behavior. They fit their model to biaxial data of a porcine aortic valve.

CONCLUSIONS

Presented here is a concise review of the computational methods and experimental studies developed for modeling of heart valves. With faster computers and more efficient numerical methods, computational modeling is becoming a mainstay in the design and development of heart valves. The advancements in experimental techniques such as particle image velocimetry and real-time imaging tools can provides avenues for validation of computational methods. Computational tools once validated with advanced experimental methods will make prediction of heart valve behavior in disease states possible. Future generation of prosthetic heart valves should also benefit with regard to design, development and testing from advanced modeling tools validated by cutting-edge experimental techniques.

ACKNOWLEDGMENTS

This review article was prepared after the Mathematics Guiding Bioartificial Heart Valve Design meeting held at the Ohio State University, October 28 to 31, 2013. The authors would like to acknowledge the Mathematical Biosciences Institute and its grant from National Science Foundation (DMS 0931642) that facilitated the meeting.

REFERENCES

[1]Affeld, K., P. Walker, and K. Schichl. The use of image processing in the investigation of artificial heart valve flow. *ASAIO J*. 35:294–297, 1989.

[2]Agathos, E. A., M. Shen, M. Katsiboulas, P. Koutsoukos, and G. Gloustianou. In vivo calcification of glutaraldehyde-fixed cardiac valve and pericardium of phoca groenlandica. *ASAIO J*. 57(328–332):3, 2011. doi: 10.1097/MAT.1090b1013e3182179a3182189.

[3]Alavi, S. H., V. Ruiz, T. Krasieva, E. Botvinick, and A. Kheradvar. Characterizing the collagen fiber orientation in pericardial leaflets under mechanical loading conditions. *Ann. Biomed. Eng*. 41:547–561, 2013.

[4]Alavi, S. H., A. Sinha, E. Steward, J. C. Milliken, and A. Kheradvar. Load-dependent extracellular matrix organization in atrioventricular heart valves: differences and similarities. *Am. J. Physiol. Heart Circ. Physiol*. 309(2):H276–H284, 2015. doi:10.1152/ajpheart.00164.2015.

[5]Alemu, Y., and D. Bluestein. Flow-induced platelet activation and damage accumulation in a mechanical heart valve: numerical studies. *Artif. Organs* 31:677–688, 2007.

[6]Amatya, D., D. Troolin, and E. Longmire. 3d3c velocity measurements downstream of artificial heart valves. *Methods* 7:9, 2009.

[7]Antman, S. S. Nonlinear Problems of Elasticity, Volume 107 of Applied Mathematical Sciences. New York: Springer-Verlag, 2005.

[8]Arjunon, S., P. H. Ardana, N. Saikrishnan, S. Madhani, B. Foster, A. Glezer, and A. P. Yoganathan. Design of a pulsatile flow facility to evaluate thrombogenic potential of implantable cardiac devices. *J. Biomech. Eng*. 137:045001, 2015.

[9]Azadani, A. N., S. Chitsaz, P. B. Matthews, N. Jaussaud, J. Leung, T. Tsinman, L. Ge, and E. E. Tseng. Comparison of mechanical properties of human ascending aorta and aortic sinuses. *Ann. Thorac. Surg*. 93:87–94, 2012.

[10]Bellhouse, B. J., and F. H. Bellhouse. Fluid mechanics of the mitral valve. *Nature* 224:615–616, 1969.

[11]Belytschko, T., W. K. Liu, B. Moran, and K. Elkhodary. Nonlinear Finite Elements for Continua and Structures. New York: Wiley, 2013.

[12]Bernacca, G. M., A. C. Fisher, T. G. Mackay, and D. J. Wheatley. A dynamic in vitro method for studying bioprosthetic heart valve calcification. *J. Mater. Sci. Mater. Med*. 3:293–298, 1992.

[13]Billiar, K. L., and M. S. Sacks. Biaxial mechanical properties of the natural and glutaraldehyde treated aortic valve cusp—part I: experimental results. *J. Biomech. Eng*. 122:23–30, 1999.

[14]Billiar, K. L., and M. S. Sacks. Biaxial mechanical properties of the natural and glutaraldehyde treated aortic valve cusp—part I: experimental results. *J. Biomech. Eng*. 122:23–30, 2000.

[15]Billiar, K. L., and M. S. Sacks. Biaxial mechanical properties of the native and glutaraldehyde-treated aortic valve cusp: Part II—a structural constitutive model. *J. Biomech. Eng*. 122:327–335, 2000.

[16]Bischoff, J. E., E. A. Arruda, and K. Grosh. A microstructurally based orthotropic hyperelastic constitutive law. *J. Appl. Mech*. 69:570–579, 2002.

[17]Bluestein, D., E. Rambod, and M. Gharib. Vortex shedding as a mechanism for free emboli formation in mechanical heart valves. *Trans. Am. Soc. Mech. Eng. J. Biomech. Eng*. 122:125–134, 2000.

[18]Boffi, D., L. Gastaldi, L. Heltai, and C. S. Peskin. On the hyper-elastic formulation of the immersed boundary method. *Int. J. Numer. Methods Biomed. Eng*. 197:2210–2231, 2008.

[19]Boloori_Zadeh, P., S. C. Corbett, and H. Nayeb-Hashemi. Effects of fluid flow shear rate and surface rough-

ness on the calcification of polymeric heart valve leaflet. *Mater. Sci. Eng. C.* 33:2770–2775, 2013.
[20]Bonet, J., and R. Wood. Nonlinear Continuum Mechanics for Finite Element Analysis. Cambridge: Cambridge University Press, 1997.
[21]Brücker, C. Dual-camera DPIV for flow studies past artificial heart valves. *Exp. Fluids* 22:496–506, 1997.
[22]Brust, M., C. Schaefer, R. Doerr, L. Pan, M. Garcia, P. Arratia, and C. Wagner. Rheology of human blood plasma: viscoelastic versus newtonian behavior. *Phys. Rev. Lett.* 110:078305, 2013.
[23]Burdon, T. A., D. C. Miller, P. E. Oyer, R. S. Mitchell, E. B. Stinson, V. A. Starnes, and N. E. Shumway. Durability of porcine valves at fifteen years in a representative north american patient population. *J Thorac Cardiovasc Surg.* 103:238–251, 1992; (discussion 251-232).
[24]Cacciola, G., G. W. M. Peters, and F. P. T. Baaijens. A synthetic fiber-reinforced stentless heart valve. *J. Biomech.* 33:653–658, 2000.
[25]Campo-Deaño, L., R. P. Dullens, D. G. Aarts, F. T. Pinho, and M. S. Oliveira. Viscoelasticity of blood and viscoelastic blood analogues for use in polydymethylsiloxane in vitro models of the circulatory system. *Biomicrofluidics.* 7:034102, 2013.
[26]Castellini, P., M. Pinotti, and L. Scalise. Particle image velocimetry for flow analysis in longitudinal planes across a mechanical artificial heart valve. *Artif. Organs* 28:507–513, 2004.
[27]Chan, V., A. Kulik, A. Tran, P. Hendry, R. Masters, T. G. Mesana, and M. Ruel. Long-term clinical and hemodynamic performance of the hancock ii versus the perimount aortic bioprostheses. *Circulation* 122:S10–S16, 2010.
[28]Chandra, S., N. M. Rajamannan, and P. Sucosky. Computational assessment of bicuspid aortic valve wall-shear stress: implications for calcific aortic valve disease. *Biomech. Model. Mechanobiol.* 11:1085–1096, 2012.
[29]Chandran, K., R. Fatemi, L. Hiratzka, and C. Harris. Effect of wedging on the flow characteristics past tilting disc aortic valve prosthesis. *J. Biomech.* 19:181–186, 1986.
[30]Cheng, R., Y. G. Lai, and K. B. Chandran. Three-dimensional fluid-structure interaction simulation of bileaflet mechanical heart valve flow dynamics. *Ann. Biomed. Eng.* 32:1471–1483, 2004.
[31]Chikwe, J., and F. Filsoufi. Durability of tissue valves. *Semin. Thorac. Cardiovasc. Surg.* 23:18–23, 2011.
[32]Dabagh, M., M. J. Abdekhodaie, and M. T. Khorasani. Effects of polydimethylsiloxane grafting on the calcification, physical properties, and biocompatibility of polyurethane in a heart valve. *J. Appl. Polym. Sci.* 98:758–766, 2005.
[33]Daily, B. B., T. W. Pettitt, S. P. Sutera, and W. S. Pierce. Pierce-donachy pediatric vad: progress in development. *Ann. Thorac. Surg.* 61:437–443, 1996.
[34]Dalmau, M. J., J. M. González-Santos, J. A. Blázquez, J. A. Sastre, J. López-Rodríguez, M. Bueno, M. Castaño, and A. Arribas. Hemodynamic performance of the medtronic mosaic and perimount magna aortic bioprostheses: five-year results of a prospectively randomized study. *Eur. J. Cardiothorac. Surg.* 39:844–852, 2011.
[35]Dasi, L., L. Ge, H. Simon, F. Sotiropoulos, and A. Yoganathan. Vorticity dynamics of a bileaflet mechanical heart valve in an axisymmetric aorta. *Phys. Fluids. (1994-present)* 19:067105, 2007.
[36]David, T. E., S. Armstrong, and M. Maganti. Hancock II bioprosthesis for aortic valve replacement: the gold standard of bioprosthetic valves durability? *Ann. Thorac. Surg.* 90:775–781, 2010.
[37]De Hart, J., F. P. T. Baaijens, G. W. M. Peters, and P. J. G. Schreurs. A computational fluid-structure interaction analysis of a fiber-reinforced stentless aortic valve. *J. Biomech.* 36:699–712, 2003.
[38]De Hart, J., G. W. Peters, P. J. Schreurs, and F. P. Baaijens. A two-dimensional fluid–structure interaction model of the aortic value. *J. Biomech.* 33:1079–1088, 2000.
[39]De Hart, J., G. Peters, P. Schreurs, and F. Baaijens. A three-dimensional computational analysis of fluid–structure interaction in the aortic valve. *J. Biomech.* 36:103–112, 2003.
[40]De Hart, J., G. Peters, P. Schreurs, and F. Baaijens. Collagen fibers reduce stresses and stabilize motion of aortic valve leaflets during systole. *J. Biomech.* 37:303–311, 2004.
[41]Donea, J., S. Giuliani, and J. Halleux. An arbitrary lagrangian-eulerian finite element method for transient dynamic fluid-structure interactions. *Comput. Methods Appl. Mech. Eng.* 33:689–723, 1982.
[42]Driessen, N. J. B., R. A. Boerboom, J. M. Huyghe, C. V. C. Bouten, and F. P. T. Baaijens. Computational analyses of mechanically induced collagen fiber remodeling in the aortic heart valve. *J. Biomech. Eng.* 125:549–557, 2003.
[43]Fai, T. G., B. E. Griffith, Y. Mori, and C. S. Peskin. Immersed boundary method for variable viscosity and variable density problems using fast constant-coefficient linear solvers I: numerical method and results. *SIAM J. Sci. Comput.* 35:B1132–B1161, 2013.
[44]Fai, T. G., B. E. Griffith, Y. Mori, and C. S. Peskin. Immersed boundary method for variable viscosity and variable density problems using fast constant-coefficient linear solvers II: theory. *SIAM J. Sci. Comput.* 36:B589–B621, 2014.
[45]Falahatpisheh, A., and A. Kheradvar. High-speed particle image velocimetry to assess cardiac fluid dynamics in vitro: from performance to validation. *Eur. J. Mech. B. Fluids* 35:2–8, 2012.
[46]Falahatpisheh, A., G. Pedrizzetti, and A. Kheradvar. Three-dimensional reconstruction of cardiac flows based on multi-planar velocity fields. *Exp. Fluids* 55:1–15, 2014.
[47]Faludi, R., M. Szulik, J. D'hooge, P. Herijgers, F. Rademakers, G. Pedrizzetti, and J.-U. Voigt. Left ventricular flow patterns in healthy subjects and patients with prosthetic mitral valves: an in vivo study using echocardiographic particle image velocimetry. *J Thorac Cardiovasc Surg.* 139:1501–1510, 2010.
[48]Fann, J. I., D. C. Miller, K. A. Moore, R. S. Mitchell, P. E. Oyer, E. B. Stinson, R. C. Robbins, B. A. Reitz, and N. E. Shumway. Twenty-year clinical experience with porcine bioprostheses. *Ann. Thorac. Surg.* 62:1301–1312, 1996.
[49]Flamini V, DeAnda A, Griffith BE. Immersed boundary-finite element model of fluid-structure interaction in the aortic root. *arXiv preprint arXiv:1501.02287.* 2015.
[50]Gao, H., X. Ma, N. Qi, C. Berry, B. E. Griffith, and X. Luo. A finite strain nonlinear human mitral valve model with fluid-structure interaction. *Int. J. Numer. Methods Biomed. Eng.* 30:1597–1613, 2014.
[51]Gao, H., H. Wang, C. Berry, X. Luo, and B. E. Griffith. Quasi-static image-based immersed boundary-finite element model of left ventricle under diastolic loading. *Int. J. Numer. Methods Biomed. Eng.* 30:1199–1222, 2014.
[52]Ge, L., L. P. Dasi, F. Sotiropoulos, and A. P. Yoganathan. Characterization of hemodynamic forces induced

by mechanical heart valves: reynolds vs. viscous stresses. *Ann. Biomed. Eng.* 36:276–297, 2008.
[53]Ge, L., H.-L. Leo, F. Sotiropoulos, and A. P. Yoganathan. Flow in a mechanical bileaflet heart valve at laminar and near-peak systole flow rates: Cfd simulations and experiments. *J. Biomech. Eng.* 127:782–797, 2005.
[54]Ge, L., and F. Sotiropoulos. A numerical method for solving the 3d unsteady incompressible navier–stokes equations in curvilinear domains with complex immersed boundaries. *J. Comput. Phys.* 225:1782–1809, 2007.
[55]Ghista, D., and A. Rao. Mitral-valve mechanics—stress/strain characteristics of excised leaflets, analysis of its functional mechanics and its medical application. *Med. Biol. Eng.* 11:691–702, 1973.
[56]Glasmacher B, Reul H, Rau G, Erckes C, Weiland J. In vitro investigation of the calcification behaviour of polyurethane biomaterials. *Polyurethanes Biomed. Eng.* II:151–168, 1986.
[57]Glowinski, R., T.-W. Pan, T. I. Hesla, and D. D. Joseph. A distributed lagrange multiplier/fictitious domain method for particulate flows. *Int. J. Multiph. Flow* 25:755–794, 1999.
[58]Griffith, B. E. Immersed boundary model of aortic heart valve dynamics with physiological driving and loading conditions. *Int. J. Numer. Methods Biomed. Eng.* 28:317–345, 2012.
[59]Griffith, B. E., R. D. Hornung, D. M. McQueen, and C. S. Peskin. Parallel and adaptive simulation of cardiac fluid dynamics. In: Advanced computational infrastructures for parallel and distributed applications, edited by M. Parashar, X. Li. pp. 105–130. 2010.
[60]Griffith, B. E., V. Flamini, A. DeAnda, and L. Scotten. Simulating the dynamics of an aortic valve prosthesis in a pulse duplicator: numerical methods and initial experience. *J. Med. Devices* 7:040912, 2013.
[61]Griffith, B. E., R. D. Hornung, D. M. McQueen, and C. S. Peskin. An adaptive, formally second order accurate version of the immersed boundary method. *J. Comput. Phys.* 223:10–49, 2007.
[62]Griffith, B. E., X. Luo, D. M. McQueen, and C. S. Peskin. Simulating the fluid dynamics of natural and prosthetic heart valves using the immersed boundary method. *Int. J. Appl. Mech.* 1:137–177, 2009.
[63]Grigioni, M., C. Daniele, G. D'Avenio, U. Morbiducci, C. Del Gaudio, M. Abbate, and D. Di Meo. Innovative technologies for the assessment of cardiovascular medical devices: state-of-the-art techniques for artificial heart valve testing. *Expert Rev. Med. Devices* 1:81–93, 2004.
[64]Grigioni, M., C. Daniele, C. Del Gaudio, A. Balducci, U. Morbiducci, G. D'Avenio, and V. Barbaro. Critical aspects for a CFD simulation compared with PIV analysis of the flow field downstream of a prosthetic heart valve. *Simulations in biomedicine* 6:271, 2003.
[65]Gross, J. M. Calcification of bioprosthetic heart valves and its assessment. *J. Thorac. Cardiovasc. Surg.* 121:428–430, 2001.
[66]Groves, E. M., A. Falahatpisheh, J. L. Su, and A. Kheradvar. The effects of positioning of transcatheter aortic valves on fluid dynamics of the aortic root. *ASAIO J.* 60:545–552, 2014.
[67]Haziza, F., G. Papouin, B. Barratt-Boyes, G. Christie, and R. Whitlock. Tears in bioprosthetic heart valve leaflets without calcific degeneration. *J. Heart Valve Dis.* 5:35–39, 1996.
[68]Hochareon, P., K. B. Manning, A. A. Fontaine, J. M. Tarbell, and S. Deutsch. Wall shear-rate estimation within the 50 cc penn state artificial heart using particle image velocimetry. *J. Biomech. Eng.* 126:430–437, 2004.
[69]Holzapfel, G. A. Nonlinear Solid Mechanics. Chichester: Wiley, 2000.
[70]Humphrey, J. D., and F. C. P. Yin. On constitutive relations and finite deformations of passive cardiac tissue: I. A pseudostrain-energy function. *J. Biomech. Eng.* 109:298–304, 1987.
[71]Jahed, Z., H. Shams, M. Mehrbod, and M. R. Mofrad. Mechanotransduction pathways linking the extracellular matrix to the nucleus. *Int. Rev. Cell Mol. Biol.* 310:171–220, 2014.
[72]Jamieson, W. R. E., L. H. Burr, A. I. Munro, and R. T. Miyagishima. Carpentier-edwards standard porcine bioprosthesis: a 21-year experience. *Ann. Thorac. Surg.* 66:S40–S43, 1998.
[73]Jamieson, W. R. E., R. Koerfer, C. A. Yankah, A. Zittermann, R. I. Hayden, H. Ling, R. Hetzer, and W. B. Dolman. Mitroflow aortic pericardial bioprosthesis—clinical performance. *Eur. J. Cardiothorac. Surg.* 36:818–824, 2009.
[74]Jamieson, W. R. E., L. J. Rosado, A. I. Munro, A. N. Gerein, L. H. Burr, R. T. Miyagishima, M. T. Janusz, and G. F. O. Tyers. Carpentier-edwards standard porcine bioprosthesis: primary tissue failure (structural valve deterioration) by age groups. *Ann. Thorac. Surg.* 46:155–162, 1988.
[75]Jorge-Herrero, E., J. M. Garcia Paez, and J. L. Del Castillo-Olivares Ramos. Tissue heart valve mineralization: review of calcification mechanisms and strategies for prevention. *J. Appl.Biomater. Biomech.* 3:67–82, 2005.
[76]Kaminsky, R., S. Kallweit, M. Rossi, U. Morbiducci, L. Scalise, P. Verdonck, and E. Tomasini. Piv measurements of flows in artificial heart valves. Particle image velocimetry. Berlin, Heidelberg: Springer, pp. 55–72, 2008.
[77]Kaminsky, R., U. Morbiducci, M. Rossi, L. Scalise, P. Verdonck, and M. Grigioni. Time-resolved PIV technique for high temporal resolution measurement of mechanical prosthetic aortic valve fluid dynamics. *Int. J. Artif. Organs* 30:153–162, 2007.
[78]Kapolos, J., D. Mavrilas, Y. Missirlis, and P. G. Koutsoukos. Model experimental system for investigation of heart valve calcification in vitro. *J. Biomed. Mater. Res.* 38:183–190, 1997.
[79]Kelley, T., S. Marquez, and C. Popelar. In vitro testing of heart valve substitutes. In: Heart Valves, edited by P. A. Iaizzo, R. W. Bianco, A. J. Hill, and J. D. St Louis. US: Springer, 2013, pp. 283–320.
[80]Kheradvar A, Groves EL, Tseng E. Foldavalve: a novel 14fr totally repositionable and retrievable transcatheter aortic valve: proof of concept in sheep. *EuroIntervention.* 10(pii):20141002–20141001, 2015.
[81]Kheradvar, A., and A. Falahatpisheh. The effects of dynamic saddle annulus and leaflet length on transmitral flow pattern and leaflet stress of a bileaflet bioprosthetic mitral valve. *J. Heart Valve Dis.* 21:225–233, 2012.
[82]Kheradvar, A., J. Kasalko, D. Johnson, and M. Gharib. An in vitro study of changing profile heights in mitral bioprostheses and their influence on flow. *ASAIO J.* 52:34–38, 2006.
[83]Kheradvar, A., M. Milano, and M. Gharib. Correlation between vortex ring formation and mitral annulus dynamics during ventricular rapid filling. *ASAIO J.* 53:8–16, 2007.
[84]Kim, H., K. B. Chandran, M. S. Sacks, and J. Lu. An experimentally derived stress resultant shell model for

heart valve dynamic simulations. *Ann. Biomed. Eng.* 35:30–44, 2007.
[85]Kim, H., J. Lu, M. S. Sacks, and K. B. Chandran. Dynamic simulation of bioprosthetic heart valves using a stress resultant shell model. *Ann. Biomed. Eng.* 36:262–275, 2008.
[86]Kim Y, Peskin CS. Penalty immersed boundary method for an elastic boundary with mass. *Physics of Fluids (1994-present)*. 19:053103, 2007.
[87]Kim Y, Zhu L, Wang X, Peskin C. On various techniques for computer simulation of boundaries with mass. In: Proceedings of the Second MIT Conference on Computational Fluid and Solid Mechanics, 2003, pp. 1746–1750.
[88]Kini, V., C. Bachmann, A. Fontaine, S. Deutsch, and J. M. Tarbell. Integrating particle image velocimetry and laser doppler velocimetry measurements of the regurgitant flow field past mechanical heart valves. *Artif. Organs* 25:136–145, 2001.
[89]Krings, M., D. Kanellopoulou, D. Mavrilas, and B. Glasmacher. In vitro ph-controlled calcification of biological heart valve prostheses. *Materialwiss. Werkstofftech.* 37:432–435, 2006.
[90]Kunzelman, K. S., and R. Cochran. Stress/strain characteristics of porcine mitral valve tissue: parallel versus perpendicular collagen orientation. *J. Card. Surg.* 7:71–78, 1992.
[91]Leo, H., L. P. Dasi, J. Carberry, H. A. Simon, and A. Yoganathan. Fluid dynamic assessment of three polymeric heart valves using particle image velocimetry. *Ann. Biomed. Eng.* 34:936–952, 2006.
[92]Kemp M. Leonardo da vinci: Experience, Experiment and Design. Princeton, NJ: Princeton University Press, 2006.
[93]Levy, R. J., F. J. Schoen, J. T. Levy, A. C. Nelson, S. L. Howard, and L. J. Oshry. Biologic determinants of dystrophic calcification and osteocalcin deposition in glutaraldehyde-preserved porcine aortic valve leaflets implanted subcutaneously in rats. *Am. J. Pathol.* 113:143–145, 1983.
[94]Li, J., X. Y. Luo, and Z. B. Kuang. A nonlinear anisotropic model for porcine aortic heart valves. *J. Biomech.* 34:1279–1289, 2001.
[95]Lighthill, S. J. Physiological Fluid Mechanics. Berlin: Springer, 1972.
[96]Lim, W. L., Y. T. Chew, T. C. Chew, and H. T. Low. Particle image velocimetry in the investigation of flow past artificial heart valves. *Ann. Biomed. Eng.* 22:307–318, 1994.
[97]Lim, W., Y. Chew, T. Chew, and H. Low. Steady flow dynamics of prosthetic aortic heart valves: a comparative evaluation with piv techniques. *J. Biomech.* 31:411–421, 1998.
[98]Lim, W., Y. Chew, T. Chew, and H. Low. Pulsatile flow studies of a porcine bioprosthetic aortic valve in vitro: Piv measurements and shear-induced blood damage. *J. Biomech.* 34:1417–1427, 2001.
[99]Linde, T., K. F. Hamilton, D. L. Timms, T. Schmitz-Rode, and U. Steinseifer. A low-volume tester for the thrombogenic potential of mechanical heart valve prostheses. *J. Heart Valve Dis.* 20:510–517, 2011.
[100]Luo, X., B. Griffith, X. Ma, M. Yin, T. Wang, C. Liang, P. Watton, and G. Bernacca. Effect of bending rigidity in a dynamic model of a polyurethane prosthetic mitral valve. *Biomech. Model. Mechanobiol.* 11:815–827, 2012.
[101]Ma, X., H. Gao, B. E. Griffith, C. Berry, and X. Luo. Image-based fluid–structure interaction model of the human mitral valve. *Comput. Fluids* 71:417–425, 2013.
[102]Mako, W. J., and I. Vesely. In vivo and in vitro models of calcification in porcine aortic valve cusps. *J. Heart Valve Dis.* 6:316–323, 1997.
[103]Manning, K. B., V. Kini, A. A. Fontaine, S. Deutsch, and J. M. Tarbell. Regurgitant flow field characteristics of the st. Jude bileaflet mechanical heart valve under physiologic pulsatile flow using particle image velocimetry. *Artif. Organs* 27:840–846, 2003.
[104]Mavrilas, D., A. Apostolaki, J. Kapolos, P. G. Koutsoukos, M. Melachrinou, V. Zolota, and D. Dougenis. Development of bioprosthetic heart valve calcification in vitro and in animal models: morphology and composition. *J. Cryst. Growth* 205:554–562, 1999.
[105]Mavrilas, D., J. Kapolos, P. G. Koutsoukos, and D. Dougenis. Screening biomaterials with a new in vitro method for potential calcification: porcine aortic valves and bovine pericardium. *J. Mater. Sci. Mater. Med.* 15:699–704, 2004.
[106]May-Newman, K., C. Lam, and F. C. Yin. A hyperelastic constitutive law for aortic valve tissue. *J. Biomech. Eng.* 131:081009, 2009.
[107]May-Newman, K., and F. C. Yin. Biaxial mechanical behavior of excised porcine mitral valve leaflets. *Am. J. Physiol. Heart Circ. Physiol.* 38:H1319, 1995.
[108]May-Newman, K., and F. C. P. Yin. A constitutive law for mitral valve tissue. *J. Biomech. Eng.* 120:38–47, 1998.
[109]McClure, R. S., N. Narayanasamy, E. Wiegerinck, S. Lipsitz, A. Maloney, J. G. Byrne, S. F. Aranki, G. S. Couper, and L. H. Cohn. Late outcomes for aortic valve replacement with the carpentier-edwards pericardial bioprosthesis: up to 17-year follow-up in 1,000 patients. *Ann. Thorac. Surg.* 89:1410–1416, 2010.
[110]McQueen, D. M., and C. S. Peskin. Computer-assisted design of butterfly bileaflet valves for the mitral position. *Scand. Cardiovasc. J.* 19:139–148, 1985.
[111]McQUEEN, D. M., C. S. Peskin, and E. L. Yellin. Fluid dynamics of the mitral valve: physiological aspects of a mathematical model. *Am. J. Physiol. Heart Circ. Physiol.* 242:H1095–H1110, 1982.
[112]Misfeld, M., and H.-H. Sievers. Heart valve macro- and microstructure. *Philos. Trans. R. Soc. B Biol. Sci.* 362:1421–1436, 2007.
[113]Mofrad, M. R., and R. D. Kamm. Cellular Mechanotransduction: Diverse Perspectives from Molecules to Tissues. Cambridge, MA: Cambridge University Press, 2009.
[114]Mol, A., N. B. Driessen, M. M. Rutten, S. Hoerstrup, C. C. Bouten, and F. T. Baaijens. Tissue engineering of human heart valve leaflets: a novel bioreactor for a strain-based conditioning approach. *Ann. Biomed. Eng.* 33:1778–1788, 2005.
[115]Morbiducci U, D Avenio G, Del Gaudio C, Grigioni M. Testing requirements for steroscopic particle image velocimetry measurements of mechanical heart valves fluid dynamics. *RAPPORTI ISTISAN*. 46:21, 2005.
[116]Mori, Y., and C. S. Peskin. Implicit second-order immersed boundary methods with boundary mass. *Comput. Methods Appl. Mech. Eng.* 197:2049–2067, 2008.
[117]Morsi, Y. S., W. W. Yang, C. S. Wong, and S. Das. Transient fluid–structure coupling for simulation of a trileaflet heart valve using weak coupling. *J. Artif. Organs.* 10:96–103, 2007.
[118]Nobili, M., U. Morbiducci, R. Ponzini, C. Del Gaudio, A. Balducci, M. Grigioni, F. M. Montevecchi, and A. Redaelli. Numerical simulation of the dynamics of a bi-

leaflet prosthetic heart valve using a fluid–structure interaction approach. *J. Biomech.* 41:2539–2550, 2008.
[119]Ogden, R. W., and G. A. Holzapfel. Mechanics of Biological Tissue. Berlin: Springer, 2006.
[120]Ogden RW. Non-linear Elastic Deformations. New York: Courier Corporation, Ellis Horwood, 1997.
[121]Othmer, H. G., F. R. Adler, M. A. Lewis, and J. C. Dallon. Case Studies in Mathematical Modeling–Ecology, Physiology, and Cell Biology. Englewood Cliffs, NJ: Prentice Hall, 1997.
[122]Patankar, N. A., P. Singh, D. D. Joseph, R. Glowinski, and T.-W. Pan. A new formulation of the distributed lagrange multiplier/fictitious domain method for particulate flows. *Int. J. Multiph. Flow* 26:1509–1524, 2000.
[123]Pereira, F., M. Gharib, D. Dabiri, and D. Modarress. Defocusing digital particle image velocimetry: a 3-component 3-dimensional dpiv measurement technique. Application to bubbly flows. *Exp Fluids.* 29:S078–S084, 2000.
[124]Peskin, C. S. Flow patterns around heart valves: a numerical method. *J. Comput. Phys.* 10:252–271, 1972.
[125]Peskin, C. S. Numerical analysis of blood flow in the heart. *J. Comput. Phys.* 25:220–252, 1977.
[126]Peskin, C. S. The immersed boundary method. *Acta numerica.* 11:479–517, 2002.
[127]Peskin, C. S., and D. M. McQueen. Modeling prosthetic heart valves for numerical analysis of blood flow in the heart. *J. Comput. Phys.* 37:113–132, 1980.
[128]Peskin, C. S., and D. M. McQueen. Mechanical equilibrium determines the fractal fiber architecture of aortic heart valve leaflets. *Am. J. Physiol. Heart Circ. Physiol.* 266:H319–H328, 1994.
[129]Pettenazzo, E., M. Deiwick, G. Thiene, G. Molin, B. Glasmacher, F. Martignago, T. Bottio, H. Reul, and M. Valente. Dynamic in vitro calcification of bioprosthetic porcine valves: evidence of apatite crystallization. *J. Thorac. Cardiovasc. Surg.* 121:500–509, 2001.
[130]Pierrakos, O., P. P. Vlachos, and D. P. Telionis. Time-resolved dpiv analysis of vortex dynamics in a left ventricular model through bileaflet mechanical and porcine heart valve prostheses. *J. Biomech. Eng.* 126:714–726, 2005.
[131]Quaini, A., S. Canic, R. Glowinski, S. Igo, C. J. Hartley, W. Zoghbi, and S. Little. Validation of a 3d computational fluid–structure interaction model simulating flow through an elastic aperture. *J. Biomech.* 45:310–318, 2012.
[132]Redaelli, A., H. Bothorel, E. Votta, M. Soncini, U. Morbiducci, Gaudio C. Del, A. Balducci, and M. Grigioni. 3-d simulation of the st. Jude medical bileaflet valve opening process: fluid-structure interaction study and experimental validation. *J. Heart Valve Dis.* 13:804–813, 2004.
[133]Rieß, F.-C., R. Bader, E. Cramer, L. Hansen, S. Schiffelers, J. Wallrath, and G. Wahl. The mosaic porcine bioprosthesis: role of age on clinical performance in aortic position. *J. Thorac. Cardiovasc. Surg.* 141(1440–1448):e1441, 2011.
[134]Riess, F.-C., E. Cramer, L. Hansen, S. Schiffelers, G. Wahl, J. Wallrath, S. Winkel, and P. Kremer. Clinical results of the medtronic mosaic porcine bioprosthesis up to 13 years. *Eur. J. Cardiothorac. Surg.* 37:145–153, 2010.
[135]Rousseau, E. P. M., A. A. van Steenhoven, J. D. Janssen, and H. A. Huysmans. A mechanical analysis of the closed hancock heart valve prosthesis. *J. Biomech.* 21:545–562, 1988.
[136]Sacks, M. S. A method for planar biaxial mechanical testing that includes in-plane shear. *J. Biomech. Eng.* 121:551–555, 1999.
[137]Sacks, M., and C. J. Chuong. Orthotropic mechanical properties of chemically treated bovine pericardium. *Ann. Biomed. Eng.* 26:892–902, 1998.
[138]Saikrishnan, N., C.-H. Yap, N. Milligan, N. Vasilyev, and A. Yoganathan. In vitro characterization of bicuspid aortic valve hemodynamics using particle image velocimetry. *Ann. Biomed. Eng.* 40:1760–1775, 2012.
[139]Schoen, F. J., G. Golomb, and R. J. Levy. Calcification of bioprosthetic heart valves: a perspective on models. *J. Heart Valve Dis.* 1:110–114, 1992.
[140]Schoen, F. J., H. Harasaki, K. M. Kim, H. C. Anderson, and R. J. Levy. Biomaterial-associated calcification: pathology, mechanisms, and strategies for prevention. *J. Biomed. Mater. Res.* 22:11–36, 1988.
[141]Schoen, F. J., and R. J. Levy. Calcification of tissue heart valve substitutes: progress toward understanding and prevention. *Ann. Thorac. Surg.* 79:1072–1080, 2005.
[142]Shandas, R., and J. Kwon. Digital particle image velocimetry (dpiv) measurements of the velocity profiles through bileaflet mechanical valves: In vitro steady. *Biomed. Sci. Instrum.* 32:161–167, 1996.
[143]Shirgaonkar, A. A., M. A. MacIver, and N. A. Patankar. A new mathematical formulation and fast algorithm for fully resolved simulation of self-propulsion. *J. Comput. Phys.* 228:2366–2390, 2009.
[144]Stella, J. A., and M. S. Sacks. On the biaxial mechanical properties of the layers of the aortic valve leaflet. *J. Biomech. Eng.* 129:757–766, 2007.
[145]Stewart, S. F., P. Hariharan, E. G. Paterson, G. W. Burgreen, V. Reddy, S. W. Day, M. Giarra, K. B. Manning, S. Deutsch, and M. R. Berman. Results of fda's first interlaboratory computational study of a nozzle with a sudden contraction and conical diffuser. *Cardiovasc. Eng. Technol.* 4:374–391, 2013.
[146]Stewart, S. F., E. G. Paterson, G. W. Burgreen, P. Hariharan, M. Giarra, V. Reddy, S. W. Day, K. B. Manning, S. Deutsch, and M. R. Berman. Assessment of cfd performance in simulations of an idealized medical device: results of fda's first computational interlaboratory study. *Cardiovasc. Eng. Technol.* 3:139–160, 2012.
[147]Stijnen, J., J. De Hart, P. Bovendeerd, and F. Van de Vosse. Evaluation of a fictitious domain method for predicting dynamic response of mechanical heart valves. *J. Fluids Struct.* 19:835–850, 2004.
[148]Sun, W., A. Abad, and M. S. Sacks. Simulated bioprosthetic heart valve deformation under quasi-static loading. *J. Biomech. Eng.* 127:905–914, 2005.
[149]Thubrikar, M. J., J. D. Deck, J. Aouad, and S. P. Nolan. Role of mechanical stress in calcification of aortic bioprosthetic valves. *J. Thorac. Cardiovasc. Surg.* 86:115–125, 1983.
[150]Thurston, G. B. Rheological parameters for the viscosity viscoelasticity and thixotropy of blood. *Biorheology.* 16:149–162, 1978.
[151]Valant, A. Z., L. Žiberna, Y. Papaharilaou, A. Anayiotos, and G. C. Georgiou. The influence of temperature on rheological properties of blood mixtures with different volume expanders—implications in numerical arterial hemodynamics simulations. *Rheol. Acta* 50:389–402, 2011.
[152]Valente, M., U. Bortolotti, and G. Thiene. Ultrastructural substrates of dystrophic calcification in porcine bioprosthetic valve failure. *Am. J. Pathol.* 119:12–21, 1985.
[153]Vesely, I., and D. Boughner. Analysis of the bending behaviour of porcine xenograft leaflets and of natural aortic valve material: bending stiffness, neutral axis and shear measurements. *J. Biomech.* 22:655–671, 1989.

[154]Vesely, I., D. Boughner, and T. Song. Tissue buckling as a mechanism of bioprosthetic valve failure. *Ann. Thorac. Surg.* 46:302–308, 1988.
[155]Webb, C. L., J. J. Benedict, F. J. Schoen, J. A. Linden, and R. J. Levy. Inhibition of bioprosthetic heart valve calcification with aminodiphosphonate covalently bound to residual aldehyde groups. *Ann. Thorac. Surg.* 46:309–316, 1988.
[156]Weinberg, E. J., and M. R. Kaazempur-Mofrad. On the constitutive models for heart valve leaflet mechanics. *Cardiovasc. Eng.* 5:37–43, 2005.
[157]Weinberg, E. J., and M. R. Kaazempur-Mofrad. A large-strain finite element formulation for biological tissues with application to mitral valve leaflet tissue mechanics. *J. Biomech.* 39:1557–1561, 2006.
[158]Weinberg, E. J., P. J. Mack, F. J. Schoen, G. García-Cardeña, and M. R. K. Mofrad. Hemodynamic environments from opposing sides of human aortic valve leaflets evoke distinct endothelial phenotypes in vitro. *Cardiovasc. Eng.* 10:5–11, 2010.
[159]Weinberg, E. J., and M. R. K. Mofrad. A finite shell element for heart mitral valve leaflet mechanics, with large deformations and 3d constitutive material model. *J. Biomech.* 40:705–711, 2007.
[160]Weinberg, E. J., and M. R. K. Mofrad. Transient, three-dimensional, multiscale simulations of the human aortic valve. *Cardiovasc. Eng.* 7:140–155, 2007.
[161]Weinberg, E. J., and M. R. K. Mofrad. A multiscale computational comparison of the bicuspid and tricuspid aortic valves in relation to calcific aortic stenosis. *J. Biomech.* 41:3482–3487, 2008.
[162]Weinberg, E. J., F. J. Schoen, and M. R. Mofrad. A computational model of aging and calcification in the aortic heart valve. *PLoS ONE* 4:e5960, 2009.
[163]Weska, R. F., C. G. Aimoli, G. M. Nogueira, A. A. Leirner, M. J. S. Maizato, O. Z. Higa, B. Polakievicz, R. N. M. Pitombo, and M. M. Beppu. Natural and prosthetic heart valve calcification: morphology and chemical composition characterization. *Artif. Organs* 34:311–318, 2010.
[164]Willert, C. E., and M. Gharib. Digital particle image velocimetry. *Exp. Fluids* 10:181–193, 1991.
[165]Wouters L, Rousseau E, Steenhoven vA, German A. An experimental set-up for the in vitro analysis of polyurethane calcification. In: Polyurethanes in biomedical engineering: II: Proceedings of the 2nd International Conference on Polyurethanes in Biomedical Engineering, Fellbach/Stuttgart, edited by H. Planck, June 18–19. vol. 3, p. 169, 1986/1987.
[166]Yin, W., Y. Alemu, K. Affeld, J. Jesty, and D. Bluestein. Flow-induced platelet activation in bileaflet and monoleaflet mechanical heart valves. *Ann. Biomed. Eng.* 32:1058–1066, 2004.
[167]Yotsumoto, G., Y. Moriyama, H. Toyohira, S. Shimokawa, Y. Iguro, S. Watanabe, H. Masuda, K. Hisatomi, and A. Taira. Congenital bicuspid aortic valve: analysis of 63 surgical cases. *J. Heart Valve Dis.* 7:500–503, 1998.
[168]Yu, Z. A dlm/fd method for fluid/flexible-body interactions. *J. Comput. Phys.* 207:1–27, 2005.
[169]Zhu, L., and C. S. Peskin. Simulation of a flapping flexible filament in a flowing soap film by the immersed boundary method. *J. Comput. Phys.* 179:452–468, 2002.